A Dual Mass Flux Framework for Boundary Layer Convection. Part I: Transport

ROEL A. J. NEGGERS,* MARTIN KÖHLER, AND ANTON C. M. BELJAARS

European Centre for Medium-Range Weather Forecasts, Reading, United Kingdom

(Manuscript received 1 October 2007, in final form 1 September 2008)

ABSTRACT

This study considers the question of what is the least complex bulk mass flux framework that can still conceptually reproduce the smoothly varying coupling between the shallow convective cloud layer and the subcloud mixed layer. To this end, the model complexity of the classic single bulk mass flux scheme is enhanced. Inspired by recent large-eddy simulation results, the authors argue that two relatively minor but key conceptual modifications are already sufficient to achieve this goal: (i) retaining a dry transporting updraft in the moist limit and (ii) applying continuous updraft area partitioning to this dual mass flux (DualM) framework. The dry updraft represents all internal mixed layer updrafts that terminate near the mixed layer top, whereas the moist updraft represents all updrafts that condense and rise out of the mixed layer as buoyant cumulus clouds. The continuous area partitioning between the dry and moist updraft is a function of moist convective inhibition above the mixed layer top. Updraft initialization is a function of the updraft area fraction and is therefore consistent with the updraft definition. It is argued that the model complexity thus enhanced is sufficient to allow reproduction of various phenomena involved in the cloud–subcloud coupling, namely (i) dry countergradient transport within the mixed layer that is independent of the moist updraft, (ii) soft triggering of moist convective flux throughout the boundary layer, and (iii) a smooth response to smoothly varying forcings, including the reproduction of gradual transitions to and from shallow cumulus convection.

The DualM framework is evaluated by implementing in the Eddy Diffusivity Mass Flux (EDMF) boundary layer scheme of the ECMWF's Integrated Forecasting System. Single column model experiments are evaluated against large-eddy simulation results for a range of different cases that span a broad parameter space of cloud–subcloud coupling intensities. The results illustrate that also in numerical practice the DualM framework can reproduce gradual transitions to and from shallow cumulus convection. Model behavior is further explored through experiments in which model complexity is purposely reduced, thus mimicking a single bulk updraft setup. This gives more insight into the new model-internal interactions and explains the obtained case results.

1. Introduction

Shallow cumulus convection plays an important role in the earth's cloud–radiative climate. Its contribution to the vertical transport of heat, moisture, and momentum away from the earth's surface has long been understood (e.g., Tiedtke 1989). Also, the typical low cloud fraction of this regime, combined with its large spatial coverage and high frequency of occurrence over subtropical oceans, significantly suppresses the shortwave cloud radiative forcing in these areas (e.g., Siebesma et al. 2004). Recently, the role of shallow cumulus convection has also been recognized in the timing of deep convective precipitation over land (e.g., Grabowski et al. 2006). Shallow cumulus convection is still a subgrid process in present-day general circulation models (GCMs) as used in numerical weather and climate prediction; whereas the dominating length scale in shallow convective transport is on the order of magnitude of 10^2 m only (Neggers et al. 2003b), the typical global GCM grid spacing is still on the order of 10^5 m. As a result, the impact of shallow cumulus convection on the larger-scale circulation and the atmosphere's water and energy budget still has to be parameterized.

For these reasons, the parameterization of shallow cumulus convection—and convection in general—has

* Current affiliation: Royal Netherlands Meteorological Institute (KNMI), De Bilt, Netherlands.

Corresponding author address: Roel A. J. Neggers, Royal Netherlands Meteorological Institute (KNMI), P.O. Box 201, De Bilt 3730 AE, Netherlands.
E-mail: roel.neggers@knmi.nl

DOI: 10.1175/2008JAS2635.1

been an active research field in recent decades. A considerable variety of methods has been developed; a recent review on convective parameterization has been written by Arakawa (2004). One method that has been particularly successful, perhaps because of its simplicity and therefore computational efficiency, is the bulk mass flux approach (Ooyama 1971; Yanai et al. 1973; Betts 1973). In this method, the vertical transport of a thermodynamic state variable ϕ, conserved for moist adiabatic motions, by a specific group of updrafts u is parameterized through a vertical advection model,

$$\overline{w'\phi'}^{u} \approx M_u(\phi_u - \bar{\phi}), \tag{1}$$

where M_u is the mass flux divided by density (hereafter referred to simply as mass flux), $\phi \in \{q_t, \theta_l\}$ (q_t is the total specific humidity and θ_l the liquid water potential temperature), and $(\phi_u - \bar{\phi})$ is the excess in ϕ of the bulk updraft over its environment. The updraft variables are obtained from a rising, entraining plume model (e.g., Simpson and Wiggert 1969). In the one extreme, (1) can be applied as a single bulk updraft model, where the model updraft represents all transporting updrafts. This is the classical application of the mass flux approach, often used in operational GCMs because of its low computational cost (e.g., Tiedtke 1989). In the other extreme, (1) is applied to many individual updrafts in the so-called ''multiple updraft'' models (e.g., Neggers et al. 2002; Cheinet 2003). These more elaborate models better resolve cumulus ensemble statistics, allowing scientific study of associated impacts on convective transport and clouds.

Large-eddy simulation (LES) of boundary layer convection has enabled the development and evaluation of parameterizations. In general, LES results support the concept of a bulk mass flux scheme. For example, Fig. 1 illustrates that moist cumulus updrafts are firmly rooted in the (subcloud) mixed layer and can be traced all the way down to the surface layer. This is consistent with the observations in nature by LeMone and Pennell (1976) and Nicholls and LeMone (1980) and supports the use of a rising plume model. Another encouraging LES result is shown in Fig. 2a; the advective mass flux model is successful in reproducing the first-order magnitude and the vertical structure of vertical convective transport in the cloud layer (Siebesma and Cuijpers 1995). Recent CRM results suggest the mass flux concept also applies to deeper convection (Kuang and Bretherton 2006).

However, other LES results have been published that question the limit of applicability of the single bulk updraft scheme. Some of these issues concern the coupling between the cloud layer and the subcloud layer; for example,

- Dry updrafts exist that never manage to condense and leave the dry mixed layer but still significantly contribute to the total turbulent flux (see Figs. 1 and 2a). It is not clear how a single bulk model updraft can simultaneously describe both very different groups of updrafts.
- The fraction of air that represents cumulus updrafts that rise out of the mixed layer is not constant in time; rather, it can vary significantly (see Fig. 2b). Although a constant fraction perhaps holds for idealized marine equilibrium situations, in highly transient continental convection it ranges from zero up to more than 5% within one diurnal cycle. Also, this variation in time is continuous and not discrete. The assumption of a constant, small area fraction is often applied in bulk mass flux schemes (e.g., Grant 2001; Soares et al. 2004).

These insights suggest that a unified representation of all encountered scenarios requires more complexity in a mass flux framework than is typically offered by a single bulk updraft scheme. On the other hand, the computational efficiency required for practical application in an operational GCM still significantly constrains model complexity. This motivates the central question asked in this study: What is the minimum level of complexity in a bulk mass flux scheme that still allows reproduction of the smoothly varying cloud–subcloud coupling that defines shallow cumulus convection? More precisely, we search for the least complex bulk mass flux framework that can still reproduce four specific concepts involved in the coupling:

- the vertical structure of transport throughout the moist convective boundary layer;
- moist convective inhibition mechanisms at cloud base;
- a smooth response to smoothly varying forcings; and
- gradual transitions to and from shallow cumulus convection.

Supported by LES results we argue that making only two relatively simple but key modifications in the standard single bulk mass flux framework is sufficient to achieve these goals. This involves increasing the number of resolved bulk updrafts from one to two and allowing the fraction of air they represent to vary in time as a continuous function of model state. As will be shown, the extra model complexity thus introduced is sufficient to effectively unify the PBL scheme while still maintaining relative simplicity in structure (and with it computational efficiency).

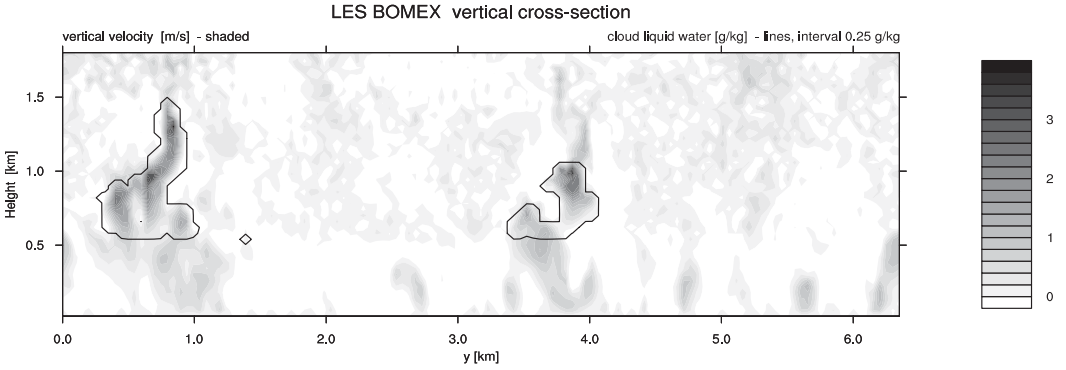

FIG. 1. A vertical cross section through an instantaneous 3D LES field of the BOMEX shallow cumulus case, showing the positive part of the vertical velocity field (gray shading) and the cloud boundaries (contour line, corresponding to 0.001 g kg^{-1} condensate).

The method of investigation is to apply the proposed modifications to an existing well-documented single bulk mass flux scheme for the convective PBL, to perform single column model (SCM) experiments for a range of relevant prototype cases, and to critically evaluate the results using LES. The new framework, here named the dual mass flux framework (DualM), can in principle be applied in any PBL scheme that features a transporting bulk updraft; the PBL scheme used in this study is the Eddy Diffusivity Mass Flux (EDMF) scheme (Siebesma and Teixeira 2000; Siebesma et al. 2007) as currently operational in the European Centre for Medium-Range Weather Forecasts (ECMWF) Integrated Forecasting System (IFS). Combining the EDMF concept with a dual mass flux framework integrates the representation of the turbulent mixed layer and the conditionally unstable cloud layer.

The LES cases referred to throughout this manuscript are described in detail in section 2. The dual mass flux framework is formulated in section 3, and its

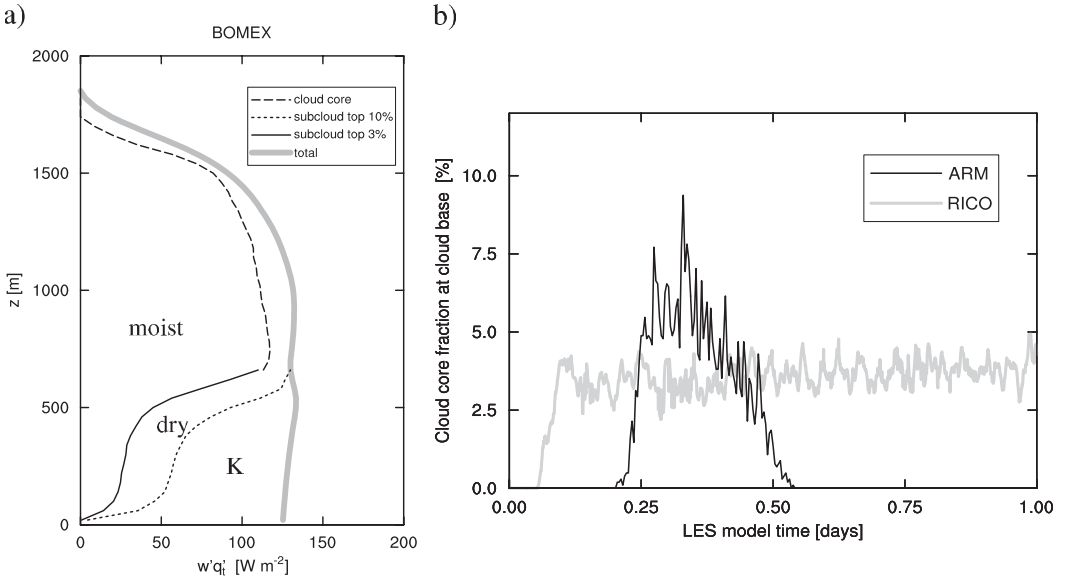

FIG. 2. LES results motivating revision of the standard single bulk mass flux framework. (a) Sampled decomposition of the turbulent flux into contributions by dry updrafts, moist updrafts, and diffusion. Above cloud base the cloud core average is plotted, defined as the area that is both cloudy and positively buoyant. Below cloud base, certain top percentages of the turbulent PDF of vertical velocity are sampled; both the top 10% and the top 3% are shown, the latter corresponding to the maximum value of the cloud core area fraction. This maximum is typically situated immediately above the mixed layer and is here used to define convective cloud base. The gray line represents the total flux. The lines represent hourly averages. (b) Time series of the cloud core area fraction at cloud base during the equilibrium RICO case and the transient ARM SGP case.

main novelties are briefly discussed in section 4. Closure of the new free model variables in the framework is described in section 5. Section 6 describes the SCM evaluation method, the results of which are presented in sections 7 and 8. This includes evaluation of mean and convective structure against LES results and the exploration of various new feedback mechanisms in the framework. Some concluding remarks can be found in section 9.

2. LES case descriptions

The central purpose of this study is to identify the least complex mass flux framework that is still able to reproduce the smoothly varying cloud–subcloud coupling typical of shallow cumulus convection. Assessment of this claim requires model evaluation for a range of different cumulus cases that together span a sufficiently broad parameter space of cloud–subcloud coupling intensities. Accordingly, the set of cases includes both transient continental scenarios, in which the coupling varies quickly, and steady-state marine cases, in which the coupling expresses an equilibrium state. The LES and SCM simulations of each case follow exactly the same settings.

Table 1 gives detailed information on all convective boundary layer cases used in this study. Most cases have been formulated by the Global Energy and Water Cycle Experiment (GEWEX) Cloud System Studies (GCSS; Browning 1993) Working Group I on boundary layer clouds. Three marine equilibrium trade wind cases are included; the Barbados Oceanographic and Meteorological Experiment (BOMEX) and Rain in Cumulus over the Ocean (RICO) cases describe Caribbean shallow cumulus, whereas the Atlantic Trade Wind Experiment (ATEX) case describes Atlantic shallow cumulus under a strong inversion. Three transient continental cumulus cases are included; the Dry Convective Boundary Layer experiment (DryCBL) case describes a deepening dry convective boundary layer, the Atmospheric Radiation Measurement Program—Southern Great Plains site (ARM SGP) case describes a diurnal cycle of shallow cumulus as observed on 21 June 1997, and the Small Cumulus Microphysics Study (SCMS) case describes a diurnal cycle of shallow cumulus as observed on 5 August 1995 at Cocoa Beach in Florida. All LES results are generated with the code of the Royal Netherlands Meteorological Institute (KNMI), described in detail by Cuijpers and Duynkerke (1993).

TABLE 1. A summary of prototype PBL cases developed for LES, documenting (in row order) (i) the case acronym, (ii) its full name, (iii) publications describing the field experiment, and (iv) publications describing the LES case setup.

ARM SGP
Atmospheric Radiation Measurement program—Southern Great Plains site
Stokes and Schwartz (1994) and Ackerman and Stokes (2003)
Brown et al. (2002)
ATEX
Atlantic Trade Wind Experiment
Augstein et al. (1973, 1974)
Stevens et al. (2001)
BOMEX
Barbados Oceanographic and Meteorological Experiment
Holland and Rasmusson (1973) and Nitta and Esbensen (1974)
Siebesma et al. (2003)
DryCBL
Dry Convective Boundary Layer experiment
Siebesma et al. (2007)
Siebesma et al. (2007)
RICO composite
Rain in Cumulus over the Ocean experiment
Rauber et al. (2007)
Van Zanten et al. (2009, manuscript submitted to *J. Atmos. Sci.*)
SCMS
Small Cumulus Microphysics Study
Knight and Miller (1998) and French et al. (1999)
Neggers et al. (2003a)

3. Framework formulation

The purpose of this section is to give a full overview of the dual mass flux framework, including its vertical structure, the basic equations, and an indication of all its elements. For clarity, no assumptions are yet made concerning the parameterization of the new free model variables in the framework (i.e., new compared to a single bulk mass flux scheme). This allows presentation of the framework as a generally applicable ''recipe'' for the parameterization of convective transport. Section 5 is exclusively dedicated to the parametric relations required for closure of the new free variables in the system.

The vertical structure of the framework is schematically illustrated in Fig. 3. Within the PBL (here defined to include the cloud layer) four layers can be distinguished: (i) a turbulent well-mixed layer of depth h, potentially topped by (ii) a convective cloud layer, with (iii) a transition layer situated in between, all (iv) capped by an inversion layer. The mixed layer depth h is estimated from the properties of a strong, nontransporting test parcel that represents the extreme of the turbulent joint probability distribution function (PDF)

$$h = \min\left(z_{\text{test}}^{\text{w=0}},\ z_{\text{test}}^{\text{lcl}}\right), \tag{2}$$

where $z_{\text{test}}^{w=0}$ is the height where the updraft vertical velocity becomes zero and $z_{\text{test}}^{\text{lcl}}$ is the updraft lifting condensation level. We here thus assume that mixed layer

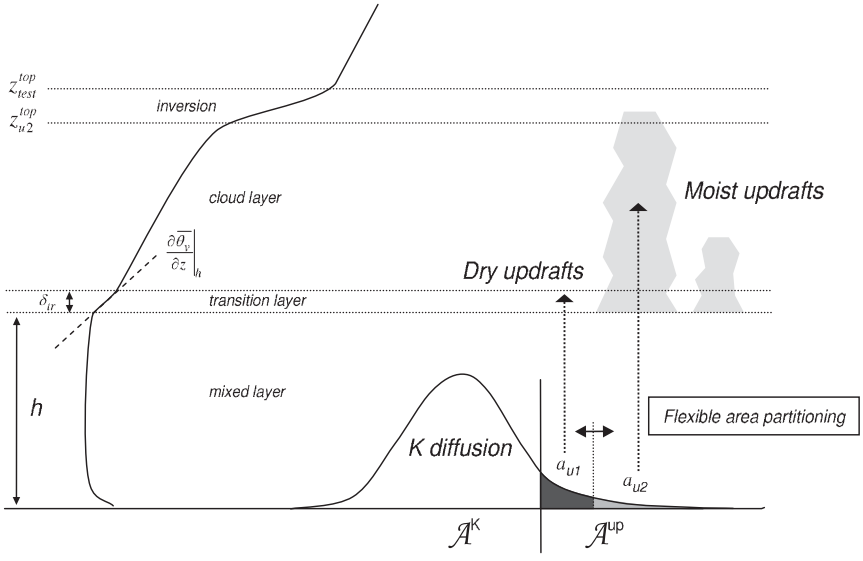

FIG. 3. A schematic illustration of the structure of the dual mass flux scheme with continuous updraft area partitioning. Various PBL layers are distinguished; mixed layer, transition layer, cloud layer, and capping inversion. Also shown is the PDF used in the surface initialization of the updrafts; $\mathcal{A}^{up} = a_{u1} + a_{u2}$ is the fraction explicitly represented by advective updrafts, whereas $\mathcal{A}^K$ represents diffusive motions. The fraction a_{u1} represents dry updrafts that never reach their lifting condensation level (shaded dark gray); fraction a_{u2} represents updrafts that condense and become positively buoyant cumulus clouds (shaded light gray).

top and convective cloud base coincide; the reason for this simplification is that the transition layer depth δ_{tr} cannot be expected to be well resolved at present-day GCMs for which this scheme is intended. Accordingly, the impact of the transition layer on transport is represented implicitly, through parameterization. Its depth is obtained from its definition as the layer in which dry mixed layer thermals that are responsible for top entrainment lose all of their kinetic energy (which scales with w_*^2) to negative buoyancy (e.g., Neggers et al. 2007):

$$\frac{g}{\Theta_0}\frac{1}{2}\frac{\partial \overline{\theta_v}}{\partial z}\bigg|_h \delta_{tr}^2 = \frac{1}{2}w_*^2, \tag{3}$$

where $w_* = (h\overline{w'B'}\big|_s)^{1/3}$ is the mixed layer convective velocity scale, with $\overline{w'B'}\big|_s$ being the surface buoyancy flux. In numerical practice, the $\overline{\theta_v}$ gradient above h can be estimated over the lowest half of the cloud layer to minimize resolution dependence. The depth δ_{tr} is used at various points in the framework.

The transport model follows the basic EDMF decomposition into an advective and diffusive flux:

$$\overline{w'\phi'} = \mathcal{A}^{up}\overline{w'\phi'}^{up} + \mathcal{A}^K\overline{w'\phi'}^K. \tag{4}$$

In standard EDMF the area fraction represented by updraft transport $\mathcal{A}^{up}$ is fixed; it is here chosen to be 10% (a maximum supported by the LES results in Fig. 2b). The single bulk advective updraft of standard EDMF is further partitioned into a dry and a moist updraft:

$$\mathcal{A}^{up}\overline{w'\phi'}^{up} = \sum_{i=1}^{2} M_{ui}(\phi_{ui} - \bar{\phi}), \tag{5}$$

where $M_{ui} = a_{ui}w_{ui}$ is the associated volumetric mass flux. The dry updraft ($i = 1$) represents all mixed layer updrafts that terminate at or in the transition layer. The moist updraft ($i = 2$) represents all updrafts that rise out of the mixed layer, condense, and continue as positively buoyant cumulus clouds (sometimes referred to as the ''cloud core''). The area fractions a_{ui} represented by each updraft are allowed to vary in time as a function of model state. The moist updraft area fraction a_{u2} is explicitly parameterized as a function of transition layer stability and proximity to saturation (to be defined in section 5). The dry updraft fraction then follows as

$$a_{u1} = \mathcal{A}^{up} - a_{u2}. \tag{6}$$

The area fractions are assumed constant with height within the mixed layer.

Updraft initialization (at the lowest model level) is made dependent on the updraft area fractions a_{ui}. The mean of a top fraction a of the joint PDF (Wyngaard

and Moeng 1992) at initialization level can be expressed as

$$\phi(a) = \bar{\phi} + \mathcal{D}(a)\sigma_\phi \quad \text{and} \tag{7}$$

$$w(a) = \mathcal{D}(a)\sigma_w, \tag{8}$$

where σ^2 is the variance at initialization level and $\mathcal{D}(a)$ is a function expressing the mean of the top fraction a of a Gaussian PDF (see Table A1 in appendix A). The variances follow the standard surface layer scaling of Wyngaard et al. (1971) and the empirical formulation of Holtslag and Moeng (1991):

$$\sigma_\phi = \frac{\overline{w'\phi'}\big|_s}{w_*} \quad \text{and} \tag{9}$$

$$\sigma_w \approx 1.2(u_*^3 + 1.5\kappa\overline{w'B'}\big|_s z^{\text{ini}})^{1/3}, \tag{10}$$

where u_* is the friction velocity, $\kappa = 0.4$ the Von Kármán constant, and z^{ini} the initialization height. The initial means of the total updraft ϕ^{up} and the moist updraft ϕ_{u2} can be obtained by substituting $\mathcal{A}^{\text{up}}$ and a_{u2} in (7) and (8), respectively. The corresponding mean of the dry updraft fraction a_{u1}, corresponding to a ''sub-top'' fraction (the dark gray shaded area in Fig. 3), can then be obtained through $\phi_{u1} = (\mathcal{A}^{\text{up}}\phi^{\text{up}} - a_{u2}\phi_{u2})/a_{u1}$. At this point the previously mentioned nontransporting test parcel, representing the extreme end of the PDF, can be defined; its fraction is here chosen as $a_{\text{test}} = 0.002$. Test parcel initialization then follows (7) and (8) as a function of a_{test}.

The updraft vertical profiles required in (5) are obtained by vertical integration of a rising plume model from these initial states. The same plume model is applied to all framework updrafts, which requires sufficient model complexity. The plume budget equations have the form proposed by Siebesma et al. (2007):

$$\frac{\partial \phi_{ui}}{\partial z} = -\epsilon_{ui}(\phi_{ui} - \bar{\phi}) + r_{ui}^{\phi}, \tag{11}$$

$$\frac{1}{2}(1 - 2\mu)\frac{\partial w_{ui}^2}{\partial z} = -b\,\epsilon_{ui}w_{ui}^2 + B_{ui} \quad \text{and} \tag{12}$$

$$B_{ui} = \frac{g}{\overline{\theta_v}}(\theta_{v,ui} - \overline{\theta_v}), \tag{13}$$

where ϵ is the lateral entrainment rate, r^{ϕ} is the impact of precipitation generation (defined in Neggers 2009, hereafter Part II), B is buoyancy, and μ and b are constants of proportionality. The principal point of departure of the above equations from those proposed by Siebesma et al. (2007) is that in our case different updrafts have different properties, reflecting different intensities of mixing with the environment; accordingly, if the plume budget model is to be applicable to all updrafts, the lateral entrainment rate ϵ_{ui} has to be allowed to depend on the state of the updraft. A closure that meets these requirements is described in section 5. Concerning the vertical extent of the updrafts, Eqs. (11)–(13) are solved where $w_{ui}^2 > 0$, so that integration terminates when $w_{ui}^2 < 0$. The dry updraft is prescribed to terminate at moist updraft cloud base, if present.

The final component to be defined is the vertical structure of the updraft mass fluxes, defined as the product of updraft fraction and updraft vertical velocity:

$$M_{ui} \equiv a_{ui}\, w_{ui}. \tag{14}$$

Within the mixed layer, the area fraction of both updrafts is assumed to be constant with height. Above h detrainment becomes significant for both bulk updrafts, and as a result the assumption of a constant updraft area fraction can no longer be maintained. The dry updraft sheds all its mass within the transition layer through a prescribed linear decrease over depth δ_{tr}. The moist updraft sheds its mass over the cloud layer by allowing its area fraction to change with height; note that this process is associated with a statistical impact on the mean properties of the bulk moist updraft. In section 5 a new parameterization is proposed for (i) the vertical structure of a_{u2} and (ii) the associated statistical correction of w_{u2} and ϕ_{u2}. Finally, similar to the dry updraft, any remaining moist mass flux at z_{u2}^{top} is linearly detrained over the capping inversion layer, here defined as the layer situated between z_{u2}^{top} and $z_{\text{test}}^{\text{top}}$, the top height of the test parcel (see also Fig. 3). Figure 4 schematically summarizes the vertical structure of the mass fluxes in the DualM scheme.

4. Interpretation

Compared to the standard single bulk mass flux framework, two key modifications have been made: (i) a dry transporting updraft is retained in the moist limit and (ii) independent closure is defined for the updraft area fraction (a continuous or ''flexible'' area partitioning). Both enhance the complexity of the PBL scheme. All other modifications (i.e., the associated added complexity in the updraft initialization, entrainment, and mass flux models) logically follow from these two key changes so that internal consistency of the framework can be maintained, and therefore by themselves the modifications do not represent major conceptual changes.

In this dual updraft system, the dry updraft is responsible for the internal mixed layer transport, whereas the

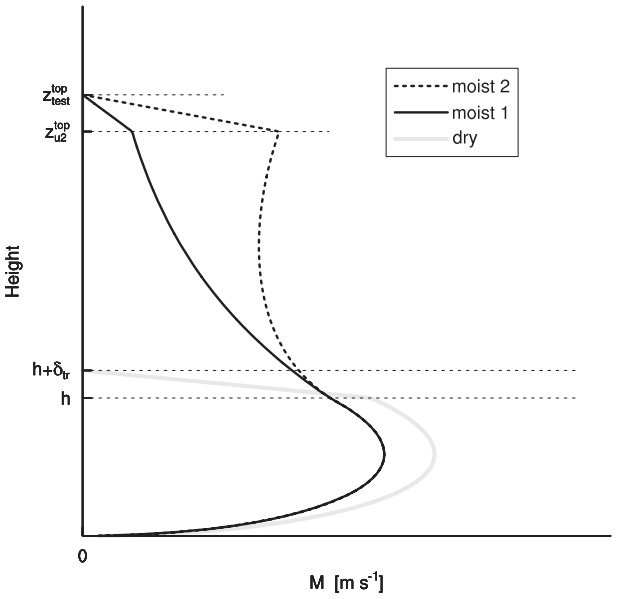

FIG. 4. A schematic illustration of the vertical structure of the updraft mass fluxes in the DualM framework, for a shallow cumulus-topped PBL. Several layers are distinguished in which the mass flux is treated differently: (i) the mixed layer (constant fraction, flexible velocity), (ii) the transition layer and inversion layer (linear decay of mass flux), and (iii) the cloud layer (flexible structure of moist mass flux; two scenarios are shown).

moist updraft represents the transport out of the mixed layer and is thus responsible for the coupling of the cloud layer with the subcloud layer. Such a system with two independently transporting updrafts has the following characteristics:

- The dry and moist updraft can coexist simultaneously in the framework; the presence of an independent, transporting dry updraft guarantees that countergradient transport always exists within the mixed layer, independent of the state of the moist updraft.
- The flux divergence at mixed layer top due to the stopping dry updraft can be effective in creating and maintaining the typically observed ''jumps'' in q_t and θ_l over the transition layer (e.g., Augstein et al. 1974; Yin and Albrecht 2000).

The main improvement is perhaps framework consistency. For example, in a two-plume model, the one-plume limit implies that the area of the second plume should be able to go to zero. Hence, the plume area should not switch between two numbers (be discrete) but should vary continuously between limits. Allowing continuous variation results in a scheme that can vary smoothly for smooth variations in the forcing. This includes gradual transitions between PBL regimes, as illustrated schematically in Fig. 5. All three major PBL regimes (i.e., the dry convective boundary layer (CBL), shallow cumulus convection, and stratocumulus convection) can in principle be represented by the dual updraft framework. On the one hand, gradual transitions to and from shallow cumulus convection are possible through the gradual introduction of a moist updraft next to an existing dry mixed layer updraft. This could be referred to as a ''soft triggering function'' for the moist convective flux. On the other hand, a gradual decoupling (in updraft sense) of a mixed layer below a cloud layer is also possible through the gradual introduction of a dry updraft next to an existing moist updraft.

Several new feedback mechanisms are introduced by the enhanced model complexity that can be distinguished a priori. First, although the two model updrafts are in principle independent (i.e., are integrated separately), they can interact indirectly through the closure of the moist updraft area fraction. The second new feedback concerns the updraft initialization; through the initial PDF closure, a larger updraft area fraction implies a smaller updraft excess and velocity and vice versa. These components thus counteract each other in the bulk flux Eq. (5); a priori it is unknown what the internal flux configuration will be when (and if) the system equilibrates. These new model-internal interactions will be further studied in the SCM evaluation.

5. Closure

The introduction of two transporting updrafts with continuous area partitioning enhances the complexity of the PBL scheme. The extra degrees of freedom require additional closure assumptions. These are (i) the moist updraft area fraction, (ii) the updraft entrainment model, and (iii) the vertical structure of cloudy mass flux. In this section three parametric relations are proposed and evaluated using LES. One functional relation is an existing formulation (lateral entrainment), one is entirely new (mass flux structure), and one is a variation on an existing formulation (area fraction).

Note that alternative, more complex closure techniques can be used instead of the ones proposed here, perhaps inspired by future insights into shallow cumulus convection. This is perfectly possible within the dual mass flux framework; it would not affect its general structure. However, as will be demonstrated, the parameterizations proposed here are successful in reproducing some key aspects of equilibrium and transient shallow cumulus convection, including some transitions to and from this regime.

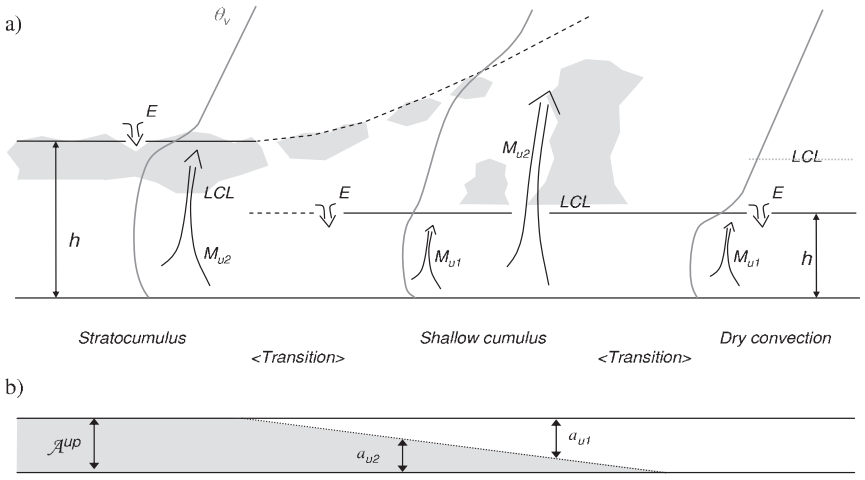

FIG. 5. (a) A schematic illustration of several typical regimes of PBL convection, and the transitions between them, that can in theory be represented by a dual mass flux framework with continuous updraft area partitioning. Included are stratocumulus (left), shallow cumulus (middle), and dry convection (right). Top entrainment E and mass flux M are shown as double arrows. (b) The corresponding partitioning of the total fraction covered by organized updrafts $\mathcal{A}^{\text{up}}$ into a dry group with fraction a_{u1} and a moist group with fraction a_{u2} (shaded).

a. Moist updraft area fraction

For the moist updraft area fraction a_{u2} we make use of the closure proposed by Neggers et al. (2007), modified as follows:

$$a_{u2} = \left(\frac{\delta}{h}\right)\frac{1}{2p+1}, \tag{15}$$

where $p = 2.2$ is a constant of proportionality obtained from LES and the depth-scale δ is taken as the minimum of transition layer depth δ_{tr} and a condensation depth-scale δ_{cl}; that is,

$$\delta = \min(\delta_{\text{tr}}, \delta_{\text{cl}}). \tag{16}$$

As shown by Neggers et al. (2007), the dependence on δ_{tr} makes the closure consistent with the Richardson-type mass flux closures as proposed by Stevens (2006) and Grant (2006) and introduces dependence on moist convective inhibition (e.g., Mapes 2000; Bretherton et al. 2004); see Eq. (3). The additional depth scale δ_{cl} reflects the requirement of updraft condensation for the occurrence of cumulus mass flux transport (e.g., Neggers et al. 2004, 2006). The sole purpose of adding this constraint is to allow the representation of a dry convective limit in the moist updraft area fraction:

$$\lim_{\delta_{\text{cl}}\to 0} a_{u2} = 0, \tag{17}$$

where δ_{cl} is assumed to be proportional to the cloudy depth of the test parcel:

$$\delta_{\text{cl}} = \gamma(z_{\text{test}}^{\text{top}} - z_{\text{test}}^{\text{lcl}}). \tag{18}$$

The constant of proportionality $\gamma = 0.15$ is calibrated to LES results (see section 8b). The dry convective limit is important for the reproduction of gradual transitions from dry to moist convection, in which the mixed layer top is initially too dry to make rising updrafts condense. The fact that condensation acts as a constraint in these transitions motivates the formulation of (16) as a minimum of two components. An attractive numerical advantage of (18) is that a_{u2} becomes dependent on a bulk property (convective cloud depth) that is well defined at the typical present-day vertical discretizations of GCMs. This will be further explored in the SCM evaluation.

b. Entrainment

The rising plume model should be applicable to all model updrafts, irrespective of the fraction that defines them. This implies that updraft lateral entrainment should be dependent on the state of the updraft. A model that meets these requirements was proposed by Neggers et al. (2002), featuring an inverse dependency on updraft vertical velocity:

$$\epsilon_{ui} = \frac{1}{\tau_\epsilon w_{ui}}. \tag{19}$$

The constant turnover time scale $\tau_\epsilon = 400$ s was diagnosed in LES. For a more thorough discussion on entrainment relations we refer to Morton et al. (1956) and Turner (1986). It is here assumed that this entrainment model also holds in the subcloud mixed layer. The vertical structure of mixed layer updraft properties as produced by this entrainment parameterization will be assessed in the SCM evaluation.

c. Mass flux structure

The parameterization of the cloud layer mass flux is inspired by the considerable difference in its vertical structure as seen in different LES cumulus cases (see Figs. 6a,b. Whereas in the RICO case the mass flux of the cloud core monotonically decreases with height, in the ATEX case it increases in the top half of the cloud layer. Also shown is q_t^x, defined as the point on the lateral mixing line between the mean state and cloud core state where $\theta_v - \overline{\theta_v} = 0$ (schematically illustrated in Fig. 6c). As suggested by De Rooy and Siebesma (2008), an interesting relation exists between the moist zero buoyancy deficit ($q_t^x - \overline{q_t}$) and the vertical structure of mass flux. This relation reflects cumulus ensemble statistics; if the mean state is further removed from moist buoyancy, a smaller fraction of cumulus updrafts manages to stay positively buoyant. The class of statistical cloud parameterizations (e.g., Sommeria and Deardorff 1977) makes use of such deficits; this motivates its application in the parameterization of the vertical structure of fraction a_{u2} in the cloud layer for use in (14).

To support the use of a statistical model we first examine in LES the general applicability of the suggested relation between the cloud core area fraction a^c and the associated normalized moist buoyancy deficit $Q^c = (q_t^x - \overline{q_t})/\sigma_{q_t}$. Because we are primarily interested in vertical structure, we express this relation in terms of normalized gradients:

$$\Gamma_a \equiv \frac{1}{a^c}\frac{\partial a^c}{\partial z'} \approx C_a \frac{1}{Q^c}\frac{\partial Q^c}{\partial z'}, \tag{20}$$

where z' is height above cloud base normalized by cloud layer depth and superscript c indicates the cloud core. Figure 7 shows the results for a range of different cumulus cases with the gradients diagnosed at every level in the cloud layer. The data collapse gives proof of principle, with constant of proportionality $C_a = -1.8$.

In practice, it is assumed for simplicity that the greatest vertical variation in Q^c is carried by the deficit (numerator) and not the variance (denominator), which is assumed to be constant. For estimation of q_t^x the lateral mixing line is reconstructed between the mean state and the test parcel state. To optimize numerical robustness, the profile of a^c is reconstructed from its gradients at the cloud layer boundaries, with the layer-internal values obtained through linear interpolation:

$$\Gamma_a(z') = (1 - z')\Gamma_a^h + z'\,\Gamma_a^{\text{top}}. \tag{21}$$

The boundary values are diagnosed as bulk gradients over the top half and bottom half of the cloud layer. The fraction a^c can thus be integrated upward from h and initialized with the constant mixed layer value of the moist updraft area fraction a_{u2}.

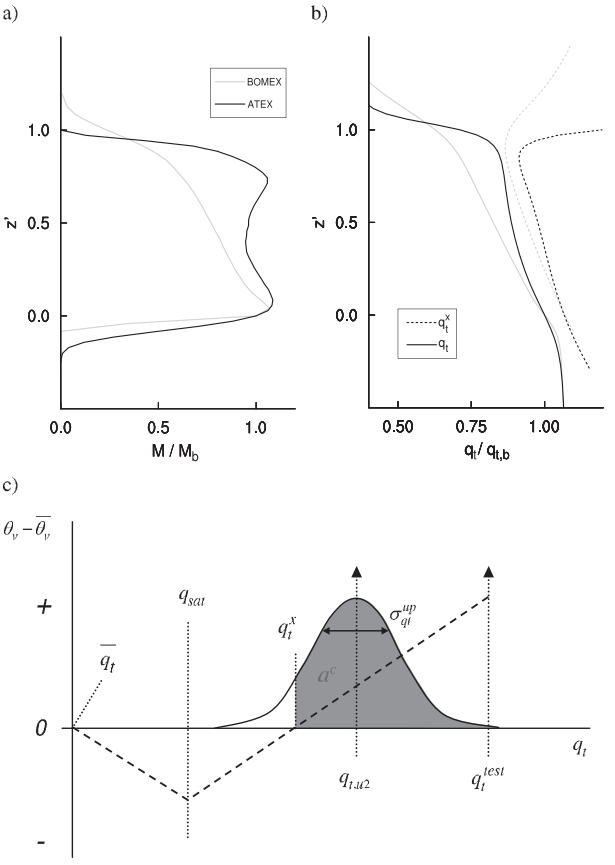

FIG. 6. The vertical structure of LES (a) cloud core mass flux and (b) mean specific humidity $\overline{q_t}$ and moist zero buoyancy point q_t^x, as sampled in RICO and ATEX; z' is height above cloud base normalized by cloud layer depth, whereas mass flux and humidity are normalized by their values at cloud base. (c) Schematic illustration of the various points on the lateral mixing line, here shown as a function of total specific humidity q_t; $\overline{q_t}$ is the horizontal mean, q_{sat} the saturation specific humidity, q_t^x the moist zero buoyancy point, $q_{t,u2}$ the moist updraft, and q_t^{test} the test parcel. The dashed line is the θ_v excess (y axis). The updraft PDF featuring in the mass flux model is also shown, of which the gray shading represents the positively buoyant fraction a^c (the cloud core).

With a^c known, the means w^c and ϕ^c can be calculated. These represent the mean properties of a^c, defined as the subset of the cloud base a_{u2} that is still positively buoyant at height z'. Accordingly, their closure should depend both on updraft ensemble statistics (i.e., a^c) and on the spread in properties over the updraft ensemble. Assuming that the moist updrafts are organized as an independent Gaussian PDF (see Fig. 6c), positioning the updraft PDF mean on the moist updraft value as given by the single plume model gives

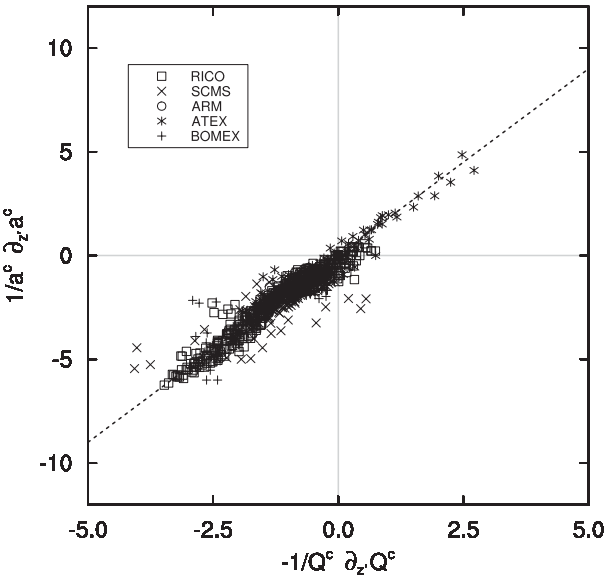

FIG. 7. The normalized gradients of a^c and Q^c as diagnosed in various LES cases. Each point represents a combination of values at a single level in an hourly averaged LES profile. The dotted line represents a linear least squares fit; the symbol type indicates the case.

$$w^c = w_{u2} + \mathcal{D}\left(\frac{a^c}{a_{u2}}\right)\sigma_w^{\mathrm{up}}, \tag{22}$$

$$\phi^c = \phi_{u2} + \mathcal{D}\left(\frac{a^c}{a_{u2}}\right)\sigma_\phi^{\mathrm{up}}, \tag{23}$$

where the updraft variance σ^{up} is obtained by tying the updraft PDF to the moist parcel and test parcel profiles:

$$\sigma_w^{\mathrm{up}} = \frac{w^{\mathrm{test}} - w_{u2}}{\mathcal{D}\left(\frac{a^{\mathrm{test}}}{a_{u2}}\right)}, \tag{24}$$

$$\sigma_\phi^{\mathrm{up}} = \frac{\phi^{\mathrm{test}} - \phi_{u2}}{\mathcal{D}\left(\frac{a^{\mathrm{test}}}{a_{u2}}\right)}. \tag{25}$$

The updraft PDF is thus reconstructed as a function of only a few single resolved parcels. In Part II this method will be further explored in the context of the parameterization of PBL cloud fraction and condensate.

What remains is to replace a_{u2}, w_{u2}, and ϕ_{u2} in (5) and (14) in the cloud layer with their c-indicated equivalents as defined above. The impact of cumulus ensemble statistics is thus represented in both the mass flux and the excesses of the bulk moist updraft in the cloud layer. In addition, the instability of the environment as felt by rising cumulus updrafts also affects the vertical structure of mass flux through the vertical structure of w^c. The performance of this scheme will be evaluated in sections 7 and 8.

6. Evaluation method

a. Implementation in IFS

For evaluation, the DualM framework is implemented into the EDMF scheme that is part of the currently operational IFS (Tompkins et al. 2004; Köhler 2005). In principle the DualM framework can be combined with any diffusion model in the context of EDMF; be it a *K*-profile method (Troen and Mahrt 1986) or a full prognostic turbulent kinetic energy (TKE) scheme (Mellor and Yamada 1974). The current IFS diffusion scheme is of the *K*-profile type with an explicit top-entrainment closure (described in appendix B). Because the conceptual modifications in the advective transport model are the central topic of this study, extensive discussions on the role of the diffusion component in EDMF go beyond the scope of this paper; we refer the reader to Siebesma et al. (2007) for an excellent review.

The DualM scheme replaces the existing IFS shallow cumulus scheme. As a result, the IFS PBL scheme now represents the dry CBL, the stratocumulus-topped PBL, and the shallow cumulus-topped PBL. The existing stratocumulus trigger function (Klein and Hartmann 1993) in IFS is maintained and superimposed on the updraft area partitioning in DualM; when the trigger criterion is met, it is prescribed that $a_{u2} = \mathcal{A}^{\mathrm{up}}$, and no dry updraft then exists. As a result, the representation of stratocumulus in IFS has not changed significantly. The remaining IFS physics are in principle unaffected.

The values of all model constants used in this implementation of the DualM scheme are summarized in appendix A (see Table A2). Sensitivity to various defining framework constants is documented in appendix C.

b. Experiment setup

The SCM simulations exactly follow the case settings as prescribed by the references in section 2. For the marine equilibrium cases the surface sensible and latent heat fluxes are always interactive, whereas for the transient cases they are prescribed. The vertical resolution of the simulation is the 91-level resolution of the operational IFS. The integration time step of all simulations is 900 s.

The results shown here concern ''dry'' runs; that is, no cloud fraction or condensate is simulated, nor is any cloud–radiative interaction present in the simulations. Also, updraft precipitation is not represented in the plume budget ($r_{ui}^{\phi} = 0$). Only the impact of condensation on updraft buoyancy is maintained. The formulation and evaluation of the boundary layer cloud scheme is presented in Part II of this study; Part I is dedicated to the new transport model for the conserved thermodynamic state variables $\phi \in \{q_t, \theta_l\}$. The relatively low cloud

fraction and precipitation rates in the cases selected for evaluation also justify this method.

7. Results

a. Mean structure

Figure 8 shows the mean thermodynamic state and turbulent flux as produced by the DualM scheme for three North Atlantic trade wind marine equilibrium cases. The main difference between these cases is the inversion strength; decreasing from right to left, it reflects the position in the low-level trade wind flow. Good agreement exists with LES with regard to (i) mixed layer depth, (ii) cloud layer depth, and (iii) the varying degrees of cloud layer conditional instability over these cases. Particularly interesting features that are reproduced are the enhanced $\overline{q_t}$ gradient immediately above mixed layer top in all cases and the close proximity to saturation near cloud layer top in the ATEX case. The reasons behind these features will be further explored in section 8. The turbulent fluxes have the right order of magnitude and vertical structure, with $\overline{w'\theta_l'}$ becoming negative in the mixed layer and $\overline{w'q_t'}$ decreasing throughout the PBL. The latter expresses the moistening by convective turbulence, which is needed to balance the prescribed larger-scale forcings. Note that the total flux is always continuous through cloud base; this suggests that good cooperation exists between the different components of the EDMF flux.

Figure 9 documents performance for two continental transient cases, DryCBL and ARM SGP. Shown are the various PBL heights in these cases; in both scenarios the deepening rate of the PBL is realistic [the LES results of Siebesma et al. (2007) indicate that the dry mixed layer should have deepened to about 1.8 km after 10 h]. The timing of convective cloud onset and disappearance in the ARM SGP is reproduced, as is the change in mixed layer deepening rate thereafter. Also note the gradual deepening of the SCM cloud layer after cloud onset, with the initially shallow cloud layer gradually deepening to about 1.5 km depth. The reproduction of these important features will also be explored in section 8.

b. Convective structure

The structure of convection in the SCM is assessed in Fig. 10, showing updraft properties in the BOMEX subcloud mixed layer. The results show that the basic behavior of updraft excesses and velocity in the mixed layer is reproduced by the lateral entrainment model. Typical features are the ''S-shaped'' q_t excess, the θ_l excess that changes sign, the approach to neutral buoyancy at the mixed-layer top, and the convex vertical structure of mixed layer w and M. The associated entrainment rate has a concave structure; this compares well to the parabolic shape proposed by Van Ulden and Siebesma (1997). Although magnitude and structure are reproduced to the first order, deviations do exist, indicating there is room for further improvement. For example, the dry updraft w is slightly overestimated near the mixed layer top; this could point at shortcomings in the rising plume model. More research is needed to make progress.

An important result is that different updraft initialization leads to different updraft profiles, particularly in w and ϵ. The reason is the positive feedback introduced by the $(\tau w)^{-1}$ lateral entrainment model; a faster rising updraft entrains less intensely, which preserves its buoyancy, which boosts its acceleration, which leads to a higher vertical velocity, and so on. As a result, the more extreme initial excesses of the stronger updrafts can be maintained at higher levels. The fact that the strong test parcel still entrains illustrates that the positive feedback stays within bounds; the $(\tau w)^{-1}$ model guarantees that some mixing will always exist.

Figure 11 shows updraft profiles in the whole BOMEX boundary layer. In the cloud layer, the bulk moist updraft profiles can directly be compared to the cloud core means as sampled in LES because of the statistical correction as a function of a^c (as described in section 5c). This process is often referred to as ''buoyancy sorting'' (e.g., Raymond and Blyth 1986; Kain and Fritsch 1990), expressing that only the positively buoyant moist updrafts remain. The results illustrate that the decreasing area fraction, increasing vertical velocity, and decreasing mass flux with height as seen in LES are reproduced. The latter result is not trivial; because the mass flux is modeled as the product of area fraction and velocity, the fine balance between the two that produces a decreasing mass flux with height has to be found. Figure 11b also illustrates to what degree the buoyancy sorting correction (as formulated in section 5c) has affected the bulk vertical velocity by showing the ''envelope'' spanned by the moist parcel and test parcel profiles. The corrected bulk profile w^c is situated in this range as a function of $\mathcal{D}(a^c)$. Because of a^c decreasing with height, the corrected bulk profile sits closer to the extreme of the PDF (the test parcel) in the top of the cloud layer. The same holds for q_t and θ_l (see Figs. 11d,e). In particular, for w^c the correction is significant; not correcting for buoyancy sorting effects would lead to an underestimation.

Figure 11f illustrates that the LES sampled flux contributions by the various EDMF components in the mixed layer are reproduced satisfactorily; the increasing moist updraft flux with height carries the S shape typical of the q_t excess, the similarly increasing dry updraft flux disappears at cloud base, and the K-diffusive contribution

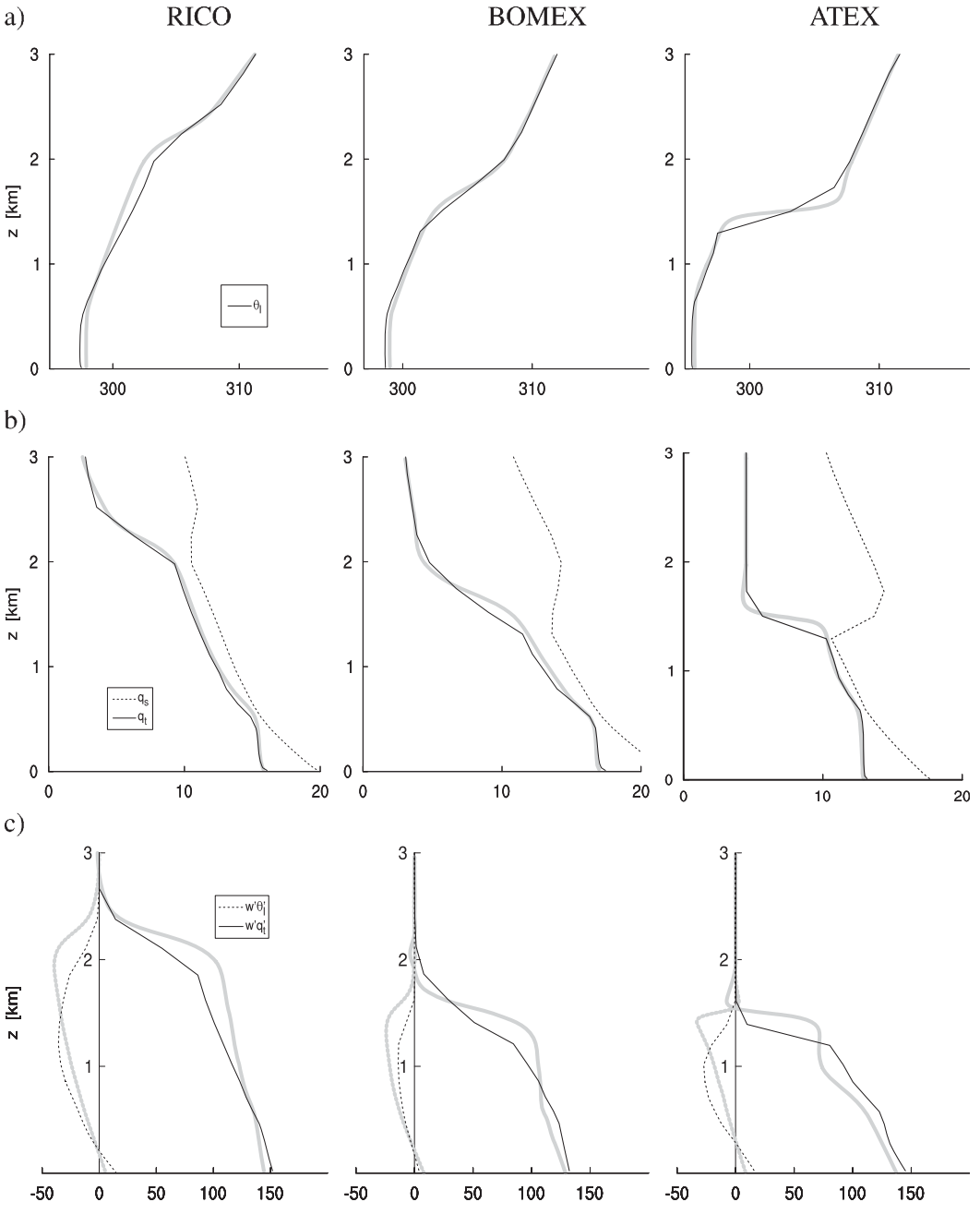

FIG. 8. The vertical profiles of mean variables for a selection of marine equilibrium cases. SCM results are plotted in black, LES in gray. Each column represents a different case, while each row represents a different variable, with (a) $\overline{\theta_l}$ (K), (b) $\overline{q_t}$ and $\overline{q_s}$ (g kg^{-1}), and (c) turbulent fluxes $\overline{w'q_t'}$ and $\overline{w'\theta_l'}$ (W m^{-2}). Each line represents a 24-h average.

fills up the remainder of the flux. In the cloud layer the whole flux is carried by the moist updraft.

A further evaluation of updraft properties is presented in Fig. 12, showing SCM versus LES scatterplots of hourly averaged moist updraft excess properties at cloud base for multiple cases. In general the points fall along one line, illustrating that the variation in cloud base properties is reproduced by the SCM. For the transient ARM SGP case this also implies that the correct time development is reproduced. Note that the marine equilibrium cases are somewhat clustered around one point; only the ARM SGP diurnal cycle case has considerable variation in updraft properties. Clearly the need for a greater diversity in convective characteristics would be desirable.

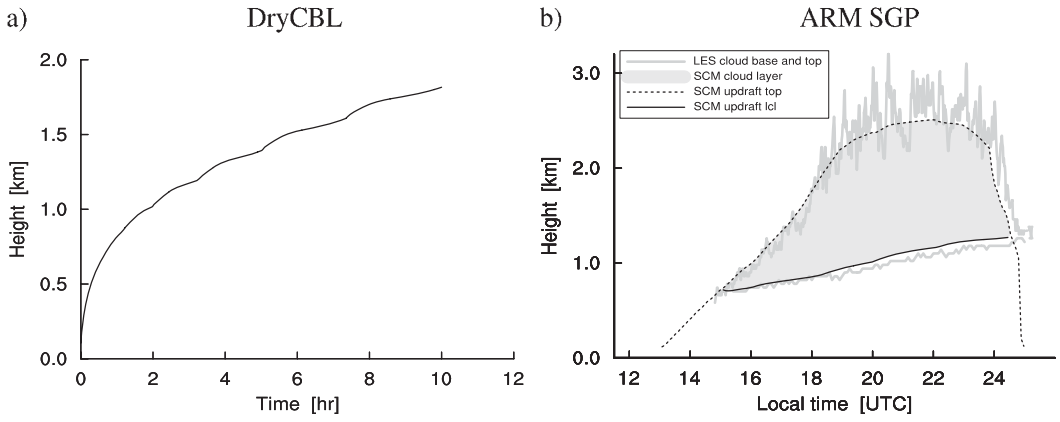

FIG. 9. The time development of the PBL during the two transient cases: (a) DryCBL and (b) ARM SGP. SCM results are plotted in black, LES results in thick gray.

8. Behavior

In this section various model-internal interactions are studied that are introduced with the dual mass flux framework. These are explored by comparing SCM experiments with the full scheme to experiments with reduced complexity, in which new components of the DualM framework are either removed or are set constant. This mimics single bulk updraft scheme settings, and the differences in results with the full DualM scheme should give more insight into the mechanics of the newly introduced model complexity. Experiments

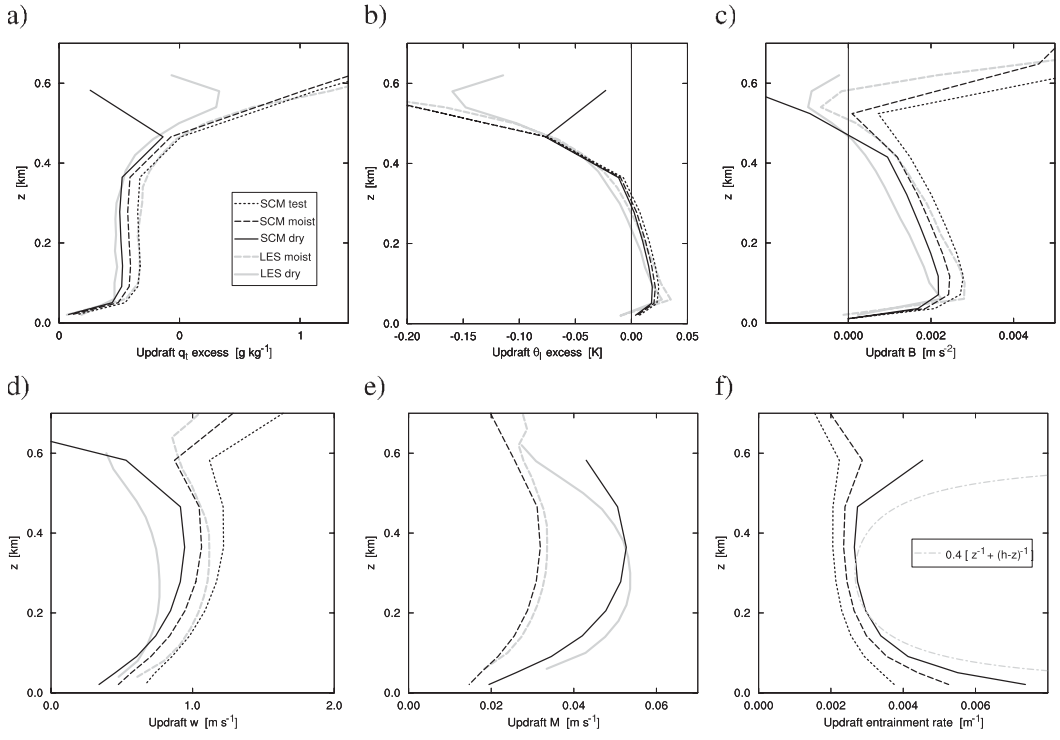

FIG. 10. The vertical profiles of updraft properties in the BOMEX subcloud layer. Shown are the excess values over the mean state of (a) q_t and (b) θ_l, (c) buoyancy B, (d) vertical velocity w, (e) mass flux M, and (f) lateral entrainment rate ϵ. All model updrafts are shown, including the dry updraft (dashed), moist updraft (solid), and test parcel (dotted). Black lines are SCM results and gray lines are LES results, except in (f) where the gray line represents the Van Ulden and Siebesma (1997) entrainment relation. Each line represents a 24-h average. Cloud base in LES BOMEX is at about 550 m.

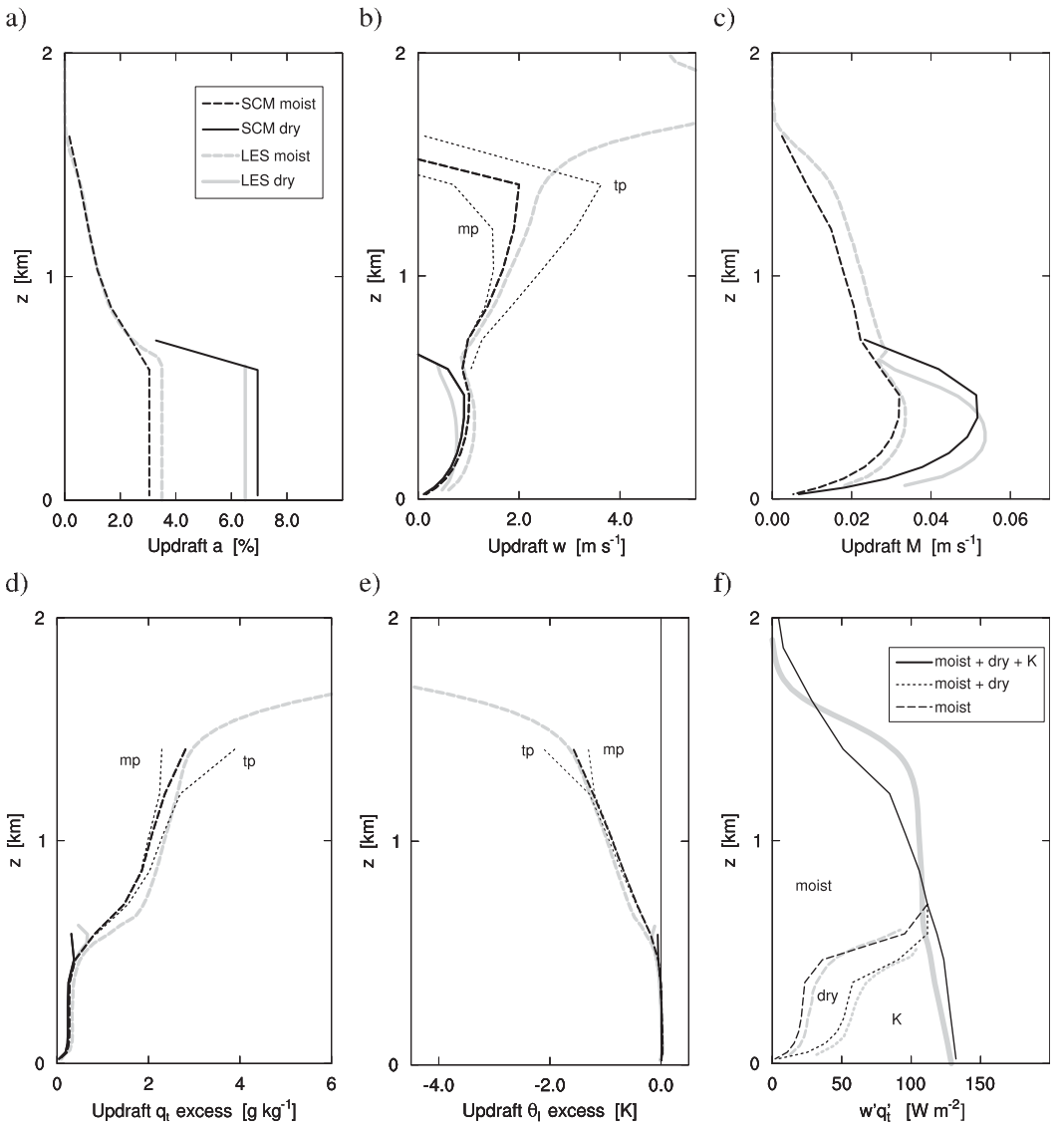

FIG. 11. As in Fig. 10, but now including the cloud layer; shown are (a) updraft area fraction, (b) updraft vertical velocity, (c) updraft mass flux, (d) updraft total specific humidity excess, and (e) updraft liquid water potential temperature excess. (f) A breakdown of the EDMF total specific humidity flux into contributions by the various components. LES results are plotted in gray; the LES cloud core is indicated by the dashed line. The thick black lines indicate transporting updraft values. In (b), (d), and (e) the thin dotted lines in the cloud layer represent the moist parcel (mp) and test parcel (tp) profiles as produced by the single plume model; these indicate the range or "envelope" in which the bulk moist updraft profile (corrected for buoyancy sorting) is situated.

with the full DualM scheme will hereafter be referred to as the "control" experiment.

a. Dry updraft

Figure 13 illustrates the impacts of dry updraft transport on subcloud mixed layer structure for the RICO case. The control experiment is compared to an experiment in which dry updraft transport is switched off ("no_dry"); only one transporting bulk updraft remains. Figure 13a shows that the full DualM scheme better reproduces the mixed layer humidity structure, in particular in the top half. The dry updraft makes the mixed layer more well mixed by picking up humidity close to the surface and depositing it near mixed layer top. As a result, $\overline{q_t}$ at mixed layer top gets closer to the saturation curve (relative humidity is higher). If clouds were simulated, this would probably boost cloud fraction at cloud base; this probable impact on clouds is explored in Part II. Figure 13b shows that the dry updraft has a similar impact on the countergradient $\overline{\theta_v}$

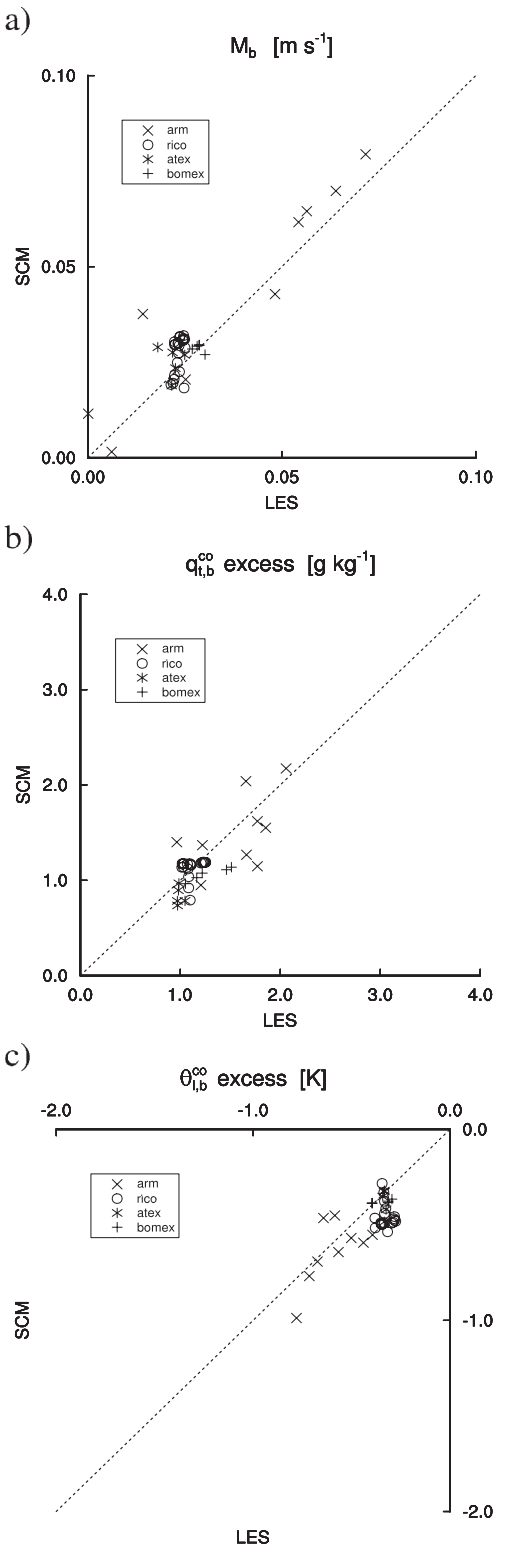

FIG. 12. SCM vs LES scatterplots of properties of the moist updraft at cloud base for a range of cases. Shown are (a) mass flux M_b, and the excesses of (b) q_t and (c) θ_l. Each point represents an hourly average; its type indicates the case.

structure of the mixed layer (Deardorff 1966; Holtslag and Moeng 1991).

b. Continuous updraft area partitioning

To illustrate the role of the continuous updraft area partitioning, the evaluation for situations with significant variation in the moist updraft area fraction is required. The first study explores the process of re-equilibration in a marine steady-state cumulus case after a perturbation; the second study explores model transience during the ARM SGP diurnal cycle of cumulus over land.

1) EQUILIBRATION

Figure 14 shows various time series of a 3-day SCM simulation of the RICO case, in which at $t = 2$ days the mean total specific humidity $\overline{q_t}$ is perturbed by $+1$ g kg^{-1} throughout the mixed layer. The results show that after the perturbation the model does not become unstable but rather smoothly re-equilibrates toward the state preceding the perturbation. The responsible negative feedback mechanism works as follows: The humidity perturbation enhances virtual potential temperature θ_v by which the θ_v jump between the mixed layer and the cloud layer decreases. Through its dependence on the transition layer depth δ_{tr}, which is a function of the $\overline{\theta_v}$ gradient above h, the fraction a_{u2} immediately responds by sharply increasing. As a result, the cloud base mass flux M_{u2} also increases, which leads to an enhanced humidity flux divergence over the mixed layer. Thus, the mixed layer starts to dry out and recover to its preperturbation state. Note that the recovery after the perturbation is smooth; Fig. 14a indicates that a continuous updraft area partitioning is required for this behavior. If the partitioning were discrete, this would lead to a discontinuous recovery.

2) TRANSIENCE

The area fraction of buoyant cumulus updrafts can vary relatively quickly during diurnal cycles of continental shallow cumulus (see, e.g., Fig. 2b). It is therefore interesting to explore the role of the continuous updraft area partitioning in the reproduction of such transient situations. Figure 15 compares the SCM results for the ARM SGP case of a control experiment with an experiment with constant $a_{u2} = 3\%$. The shallow cumulus capped mixed layer deepens significantly faster in the constant a_{u2} experiment (Fig. 15a). The reason is that the transition of moist updraft area fraction through cloud onset is discontinuous (Fig. 15b); as a result the cloud base mass flux is overestimated immediately after cloud onset (Fig. 15c), which then leads to overestimated vertical

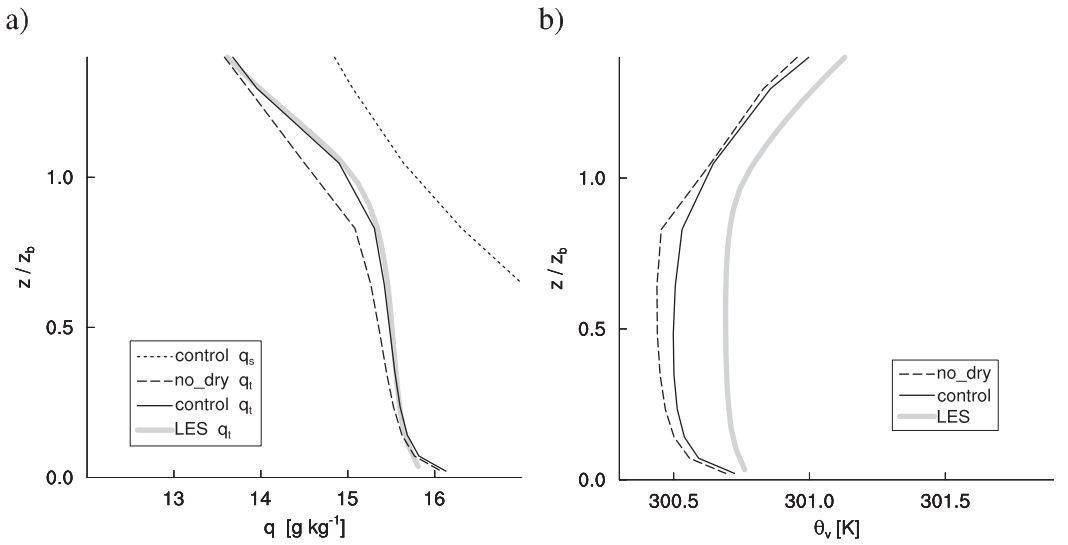

FIG. 13. Impacts of dry updraft transport on mixed layer countergradient structure and cloud base relative humidity during the RICO case: (a) total specific humidity $\overline{q_t}$; (b) virtual potential temperature $\overline{\theta_v}$. Two SCM experiments are shown: the control experiment (solid) and an experiment without dry updraft transport (dashed). Height is normalized by mixed layer depth. LES results are plotted in thick gray. In (a) the saturation specific humidity profile of the control run is also included (dotted).

mixing and too fast deepening. In contrast, because of the continuous updraft area partitioning, the onset of moist mass flux is also continuous and smooth in the control experiment.

Apparently the impact of the area fraction on mass flux is significant in such situations, and the capability to reproduce small moist updraft area fractions is important. The mechanism that initially suppresses a_{u2} is represented through its parameterization as a function of two depth scales as defined by (16); $\delta_{\rm tr}$ reflects dry top entrainment intensity and $\delta_{\rm cl}$ reflects the degree of condensation of the PDF of rising updrafts. Figure 15d shows that the order of magnitude and time development of both depth scales as diagnosed in LES is reproduced. Initially $\delta_{\rm cl}$ is zero, reflecting that no mixed layer updraft reaches condensation. Immediately after cloud onset, $\delta_{\rm cl}$ still constrains a_{u2}, reflecting that only a few updrafts yet condense above h. When the mixed layer top has approached saturation closely enough for more rising updrafts to condense, a_{u2} can become larger. Figure 15b shows that this parameterization well explains the development of the cloud base core fraction as observed in LES. The slight difference in development between a_{u2} and $\delta_{\rm cl}$ is explained by mixed layer depth h, appearing as the numerator in (15).

c. Updraft initialization

In the updraft initialization scheme [(7) and (8)], the initial updraft excess is a function of the updraft area fraction; statistically, a smaller a_{u2} implies a larger w_{u2} and ϕ_{u2} excess, and vice versa. These components thus counteract each other in the mass flux approach (5); what the impact is of this interaction is not yet clear. To gain insight into this interaction, the moist updraft initial values are studied during the ARM SGP case (see Fig. 16). The control experiment is again compared to the constant a_{u2} experiment. This illustrates that the small moist updraft area fraction at convective cloud onset and disappearance significantly enhances the initial vertical velocity (Fig. 16a) and thermodynamic excesses (Fig. 16c). Nevertheless, the associated mass flux (Fig. 16b) and total flux (Fig. 16d) always reduce to zero in the limit $a \rightarrow 0$; in other words, the fraction always overcomes the excesses. This illustrates that for reproduction of a continuous transition from dry to moist convection, a varying and continuous moist updraft area fraction is prerequisite. With a constant fraction, a flux discontinuity already exists at the lowest model level and also persists at higher levels (e.g., $z = h/2$; see Fig. 16d).

d. Mass flux structure

The mass flux closure is now examined for the ATEX case. The control experiment is compared to an experiment with a fixed, monotonically decreasing mass flux structure, considered typical for fair-weather cumulus (e.g., Siebesma and Cuijpers 1995). Figure 17 shows that with the fixed mass flux structure, $\overline{q_t}$ and M decrease too

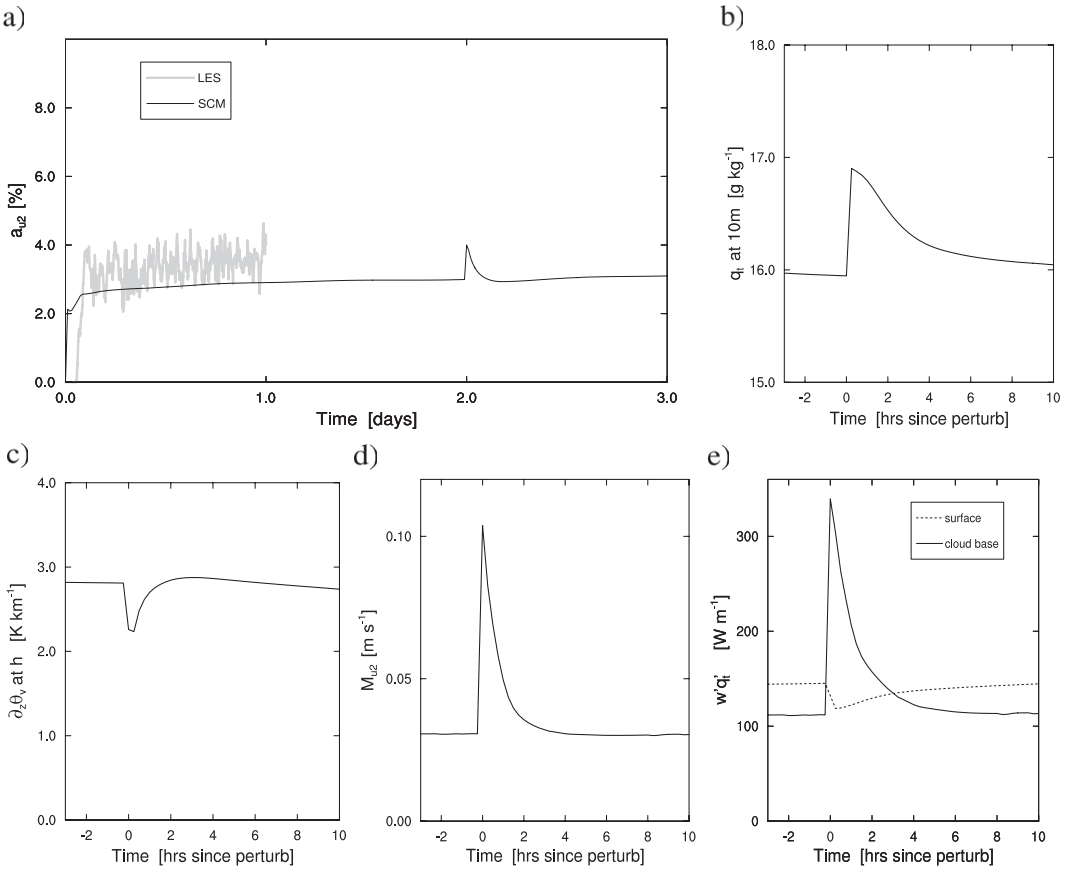

FIG. 14. Impacts of the continuous updraft area partitioning on model equilibration during the RICO case. Shown are (a) moist updraft area fraction a_u2, (b) mean total specific humidity $\overline{q_t}$ at 10 m, (c) the transition layer $\overline{\theta_v}$ gradient, (d) moist updraft mass flux at cloud base M_{u2}, and (e) total specific humidity flux $\overline{\omega' q_t'}$ at cloud base and the surface. LES results (only available for the first day) are plotted in thick gray.

much over the top half of the cloud layer. In contrast, the control experiment produces steeper gradients that better resemble LES. This indicates that the mass flux closure introduces an interaction between the mass flux and the environmental humidity (Derbyshire et al. 2004) that can be explained as follows. The relatively strong capping inversion of the ATEX case suppresses vertical mixing out of the PBL. As a result, humidity can easily accumulate immediately below the PBL top. When the saturation deficit ($q_{\text{sat}} - \overline{q_t}$) decreases, the moist zero buoyancy deficit ($q_t^x - \overline{q_t}$) also decreases (see the mixing line diagram in Fig. 6c). Through (20), this suppresses the detrainment of moist updraft mass, which enhances vertical convergence of humidity flux even further. This continues until a balance is reached between top entrainment of dry tropospheric air and the convective humidity supply from below. This interaction between environmental humidity and mass flux structure is thus self supporting, able to generate and maintain the steeper specific humidity gradients and concave mass flux structures typically observed below stronger inversions.

9. Concluding remarks

The aim of this study was to identify the simplest bulk updraft framework that is still able to reproduce the smoothly varying cloud–subcloud coupling that defines shallow cumulus convection. Supported by LES results, we argue that a dual mass flux framework, combined with continuous updraft area partitioning, should in theory already be complex enough to achieve this goal, which thus effectively unifies the representation of convective PBL transport. Compared to the single updraft scheme, the following features can now be reproduced:

- independent dry countergradient transport within a mixed layer that is capped by a cumulus cloud layer;
- continuous, potentially gradual transitions between various regimes of PBL convection due to the soft triggering of the moist convective flux;

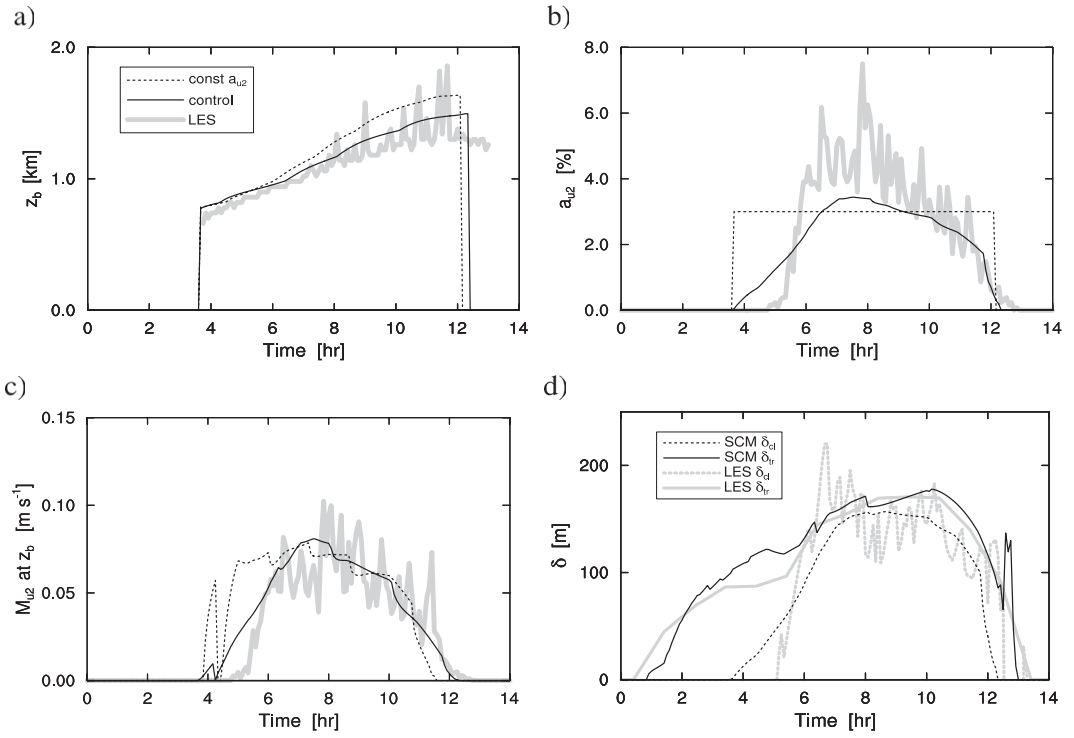

FIG. 15. Impacts of the continuous updraft area partitioning on model transience during the ARM SGP case: (a) cloud base height, (b) moist updraft area fraction at cloud base, and (c) cloud base mass flux of the moist updraft. In (a)–(c), two SCM experiments are shown; one with flexible a_{u2} (solid line), the other with constant $a_{u2} = 0.03$ (dotted). The LES lines (thick gray) represent cloud core properties at cloud base, here defined as the height of maximum cloud core fraction. (d) The transition layer depth scales δ_{tr} and δ_{cl} of the control experiment. The LES equivalent of δ_{tr} is obtained by sampling the required terms in (3), while the LES equivalent of δ_{cl} is sampled as the height difference between the level of maximum core fraction and the level of minimum buoyancy flux.

- a smooth response to smooth changes in forcing; and
- the representation of moist convective inhibition effects through the closure of the moist updraft area fraction.

The SCM evaluation of the implemented DualM scheme in the IFS for a set of different scenarios illustrates that these features can indeed be reproduced in practice, at operational NWP resolution. To this end, closures for the various new model variables were introduced, which proved effective in introducing the required complexity and the direction of model-internal feedback mechanisms. The sensitivity of model outcome for various parametric constants of proportionality was documented.

More complexity can be included into the DualM framework through more complex closures. Such models can, and probably should, be more accurate in reproducing the observed physics and behavior of shallow cumulus because they can in principle capture higher-order complexity. For example, the stratocumulus to shallow cumulus decoupling process in this implementation of EDMF–DualM still depends on observed climatology and should be improved. Another interesting question is the performance of DualM for the transition from shallow to deep convection. These topics are considered future research opportunities.

The EDMF framework with the DualM scheme offers opportunities for the statistical modeling of boundary layer clouds. The decomposition of transport into an updraft PDF and diffusive PDF that defines EDMF could similarly be applied to the PDF used to model cloud fraction and condensate. Using the same decomposition in both subgrid transport and clouds would make their representation internally consistent; for example, the updraft PDF as already defined for the mass flux model could also be used in the cloud model, by which the cloud and transport state would all be derived from the same reconstructed PDF. Second, passive (stratiform) and active (updraft) clouds would be represented independently, which has its own benefits. The opportunities thus created are explored in Part II of this study.

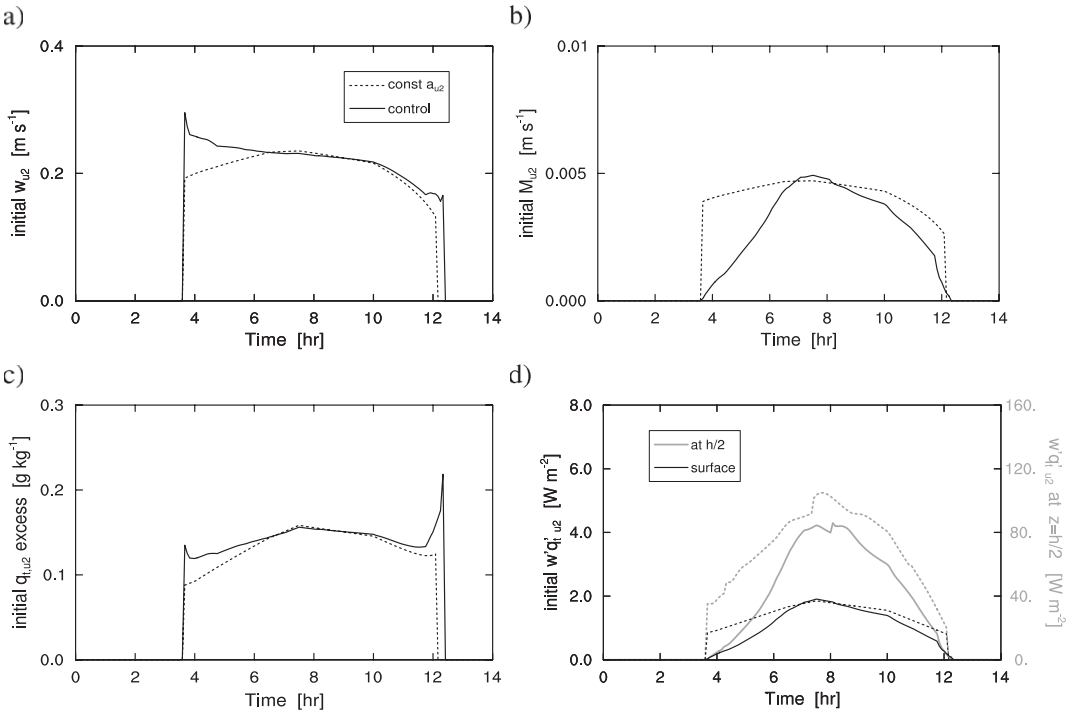

FIG. 16. As in Fig. 15, but now showing impacts of continuous updraft area partitioning on updraft surface initialization during the ARM SGP case. Shown are the initialization values of the moist updraft of (a) vertical velocity w_{u2}, (b) mass flux M_{u2}, (c) the $q_{t,\,u2}$ excess, and (d) the associated advective flux $\overline{\omega' q'_{tu2}}$. In (d) the flux at the middle of the mixed layer is also plotted (gray; right axis).

Acknowledgments. While affiliated at ECMWF, the first author was sponsored by the Atmospheric Radiation Measurement (ARM) Program of the United States Department of Energy (DOE). We thank Pier Siebesma and Philippe Bougeault for their insightful comments on early versions of this manuscript. Furthermore, we thank Geert Lenderink and Wim de Rooy for the many discussions during the development of this model and Margreet van Zanten for kindly providing the LES data on the RICO case. We thank various members of the staff at ECMWF for their generous support during this study. Finally, we thank Bjorn Stevens

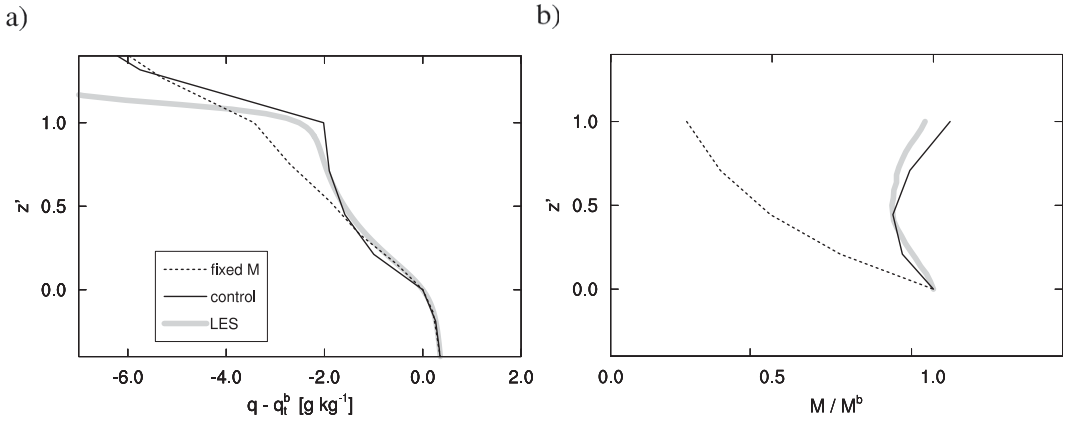

FIG. 17. Impacts of flexible cloud layer mass flux structure during the ATEX case. Shown are vertical profiles of (a) mean total specific humidity $\overline{q_t} - \overline{q_{tb}}$ and (b) the moist updraft mass flux normalized by its cloud base value, $M_{u2}/M_{u2,\,b}$. Height above cloud base is normalized by cloud layer depth. Two experiments are included; the control experiment (solid black) and the experiment with a fixed mass flux profile in the cloud layer (fixed M).

TABLE A1. The function $\mathcal{D}(a)$ expressing the mean of the top segment with area fraction a of the normal distribution $N(\overline{\phi} = 0, \sigma_\phi = 1)$.

A	$\mathcal{D}(a)$	a	$\mathcal{D}(a)$
10^{-4}	3.958	0.1	1.754
10^{-3}	3.368	0.2	1.400
0.01	2.673	0.3	1.159
0.02	2.425	0.4	0.966
0.03	2.267	0.5	0.798
0.04	2.153	0.6	0.644
0.05	2.062	0.7	0.497
0.06	1.985	0.8	0.350
0.07	1.918	0.9	0.195
0.08	1.859	0.999	0.003
0.09	1.804	1.	0

and three anonymous reviewers for their constructive comments, which we feel significantly improved both the presentation and the content of this study.

APPENDIX A

Model Constants and Precalculated Functions

Table A1 contains a range of values of the function $\mathcal{D}$, representing the mean of the fraction a of a top segment of the normal distribution. The values are calculated using the normal probability function,

$$P(x) = \frac{1}{\sigma_x\sqrt{2\pi}} e^{\left[-\frac{1}{2}\left(\frac{x-\bar{x}}{\sigma_x}\right)^2\right]}, \tag{A1}$$

with $\bar{x} = 0$ and $\sigma_x = 1$. In the PBL scheme, interpolation is used to estimate the in-between values.

The values of all model constants as applied in this implementation of the DualM scheme are summarized in Table A2.

TABLE A2. A summary of constants of proportionality in the DualM framework.

Model constant	Value	Unit
A^{up}	10	%
a^{test}	0.2	%
P	2.2	—
C_δ	0.15	—
τ_E	400	s
b	0.5	—
μ	0.15	—
C_a	−1.8	—

APPENDIX B

Implementation Details

The diffusive transport model as used in this study is in principle equivalent to that described in the IFS CY31R1 documentation ''Part IV: Physical processes'' (available online at http://www.ecmwf.int/research/ifsdocs/). Summarizing, the downgradient diffusive flux of EDMF is written as

$$\overline{w'\phi'}^K = -K_\phi \frac{\partial\overline{\phi}}{\partial z}, \tag{B1}$$

where K_ϕ is the eddy diffusivity coefficient, parameterized using prescribed profiles within the mixed layer. One mode reflects surface-driven turbulence (Troen and Mahrt 1986); the other reflects cloud top cooling-driven turbulence (Lock et al. 2000). At the tops of both bulk layers within the PBL (i.e., the mixed layer and, if present, the convective cloud layer), the entrainment flux is explicitly parameterized, there replacing (B1):

$$\overline{w'\phi'}^K_{\text{top}} = w_e\Delta\phi, \tag{B2}$$

where Δ indicates a difference across the interface and w_e is the top-entrainment velocity, parameterized as the ratio of a buoyancy flux $\overline{w'\theta'_v}$ to a buoyancy jump $\Delta\theta_v$:

$$w_e = A\frac{\overline{w'\theta'_v}}{\Delta\theta_v}. \tag{B3}$$

At the mixed layer top, $\overline{w'\theta'_v}|_s$ and $A^h = 0.2$ (e.g., Stevens 2006) are used; at cloud top, $A^{\text{cu}} = 0.4$ and the cloud layer average buoyancy flux $\langle\overline{w'\theta'_v}\rangle$ are used, as suggested by Wyant et al. (1997). For simplicity, no diffusive transport is modeled within the cumulus cloud layer.

Some numerical details remain to be stated, required for an exact reproduction of the presented results. First, to avoid double counting, the eddy diffusivity coefficients are corrected (reduced) for the fact that the top fraction $\mathcal{A}^{\text{up}}$ of the turbulent PDF is already represented by the mass flux model (described in detail in the IFS documentation). Second, again following the current numerical implementation of EDMF in IFS, in the top model layer of the PBL all mass flux is set to zero; only diffusive mixing there exists. This is motivated by the purely numerical argument that at coarse vertical discretizations the diffusive mixing model in practice better maintains strong inversions. Third, the numerical solver of EDMF exactly follows Siebesma et al. (2007), applied to the combined (mass) flux by the two updrafts. Finally, if the parameterized transition layer thickness (3) is shallower than the cloud base model layer, the dry updraft detrains all its mass in that layer.

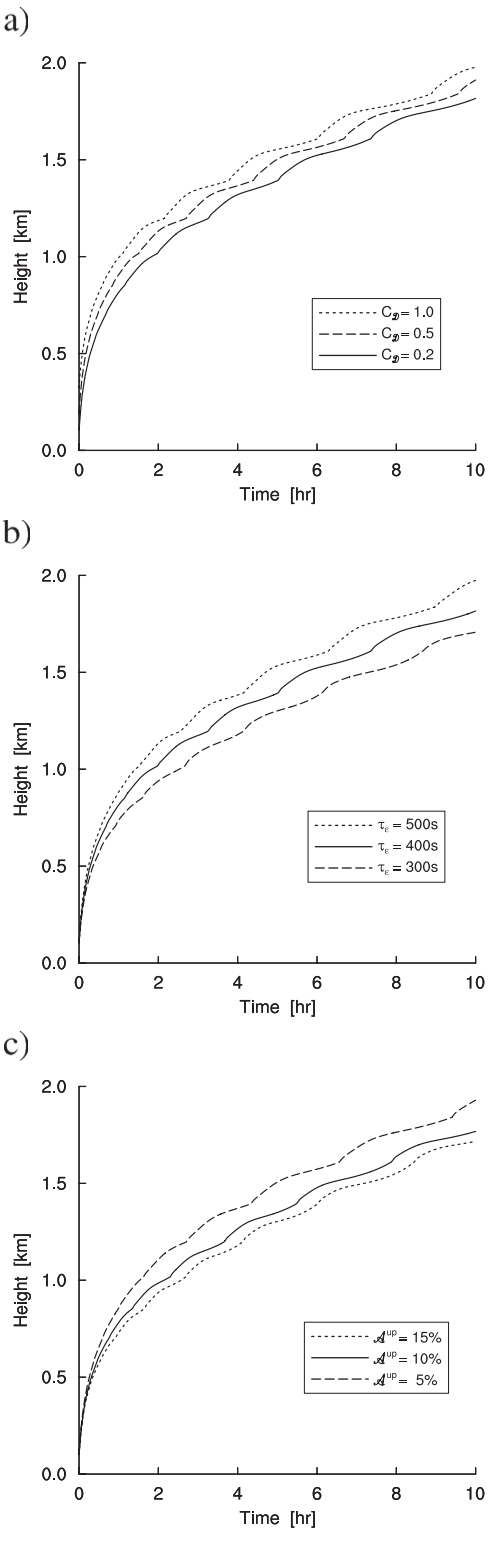

FIG. C1. The sensitivity of mixed layer deepening in the DryCBL case to (a) updraft initialization PDF factor $C_{\mathcal{D}}$, (b) updraft entrainment time scale τ_ϵ, and (c) total updraft area fraction $\mathcal{A}^{up}$. Shown is the interpolated height where the dry updraft velocity w_{u1} becomes zero. The control experiment is always plotted as a solid line.

APPENDIX C

Sensitivity to Model Constants

Figure C1 documents the sensitivity of model outcome to various model components in the updraft mass flux framework. The varied constants are (i) a factor $C_{\mathcal{D}}$ inserted into the initial updraft excesses in (7) and (8), (ii) lateral entrainment time scale τ_ϵ, and (iii) total updraft area fraction $\mathcal{A}^{up}$. All figures show the impact on the PBL deepening rate during the DryCBL case. In general, a stronger dry updraft enhances the mixed layer deepening rate. This can be achieved through a larger initial excess ($C_{\mathcal{D}}$) or a smaller entrainment rate (τ_ϵ). This sensitivity illustrates that the dry updraft affects the effective top entrainment rate of the mixed layer by preconditioning the transition layer. The diffusive and advective models thus both contribute to top entrainment; accordingly, their relative contributions should be carefully balanced. How this can consistently best be achieved is a topic of ongoing research. Note that the impact of $\mathcal{A}^{up}$ reflects two counteracting impacts on transport; a smaller $\mathcal{A}^{up}$ is associated with a larger initial updraft excess and vertical velocity, but by itself it acts to suppress the updraft mass flux. In this range of $\mathcal{A}^{up}$ values, the impact of the excess and vertical velocity dominate.

REFERENCES

Ackerman, T. P., and G. M. Stokes, 2003: The Atmospheric Radiation Measurement program. *Phys. Today,* **56,** 38–44.

Arakawa, A., 2004: The cumulus parameterization problem: Past, present, and future. *J. Climate,* **17,** 2493–2525.

Augstein, E., H. Riehl, F. Ostapoff, and V. Wagner, 1973: Mass and energy transports in an undisturbed Atlantic trade-wind flow. *Mon. Wea. Rev.,* **101,** 101–111.

——, H. Schmidt, and V. Wagner, 1974: The vertical structure of the atmospheric planetary boundary layer in undisturbed trade winds over the Atlantic Ocean. *Bound.-Layer Meteor.,* **6,** 129–150.

Betts, A. K., 1973: Non-precipitating cumulus convection and its parameterization. *Quart. J. Roy. Meteor. Soc.,* **99,** 178–196.

Bretherton, C. S., J. R. McCaa, and H. Grenier, 2004: A new parameterization for shallow cumulus convection and its application to marine subtropical cloud-topped boundary layers. Part I: Description and 1D results. *Mon. Wea. Rev.,* **132,** 864–882.

Brown, A. R., and Coauthors, 2002: Large-eddy simulation of the diurnal cycle of shallow cumulus convection over land. *Quart. J. Roy. Meteor. Soc.,* **128,** 1075–1093.

Browning, K. A., 1993: The GEWEX Cloud System Study (GCSS). *Bull. Amer. Meteor. Soc.,* **74,** 387–399.

Cheinet, S., 2003: A multiple mass-flux parameterization for the surface-generated convection. Part I: Dry plumes. *J. Atmos. Sci.,* **60,** 2313–2327.

Cuijpers, J. W. M., and P. G. Duynkerke, 1993: Large eddy simulation of trade wind cumulus clouds. *J. Atmos. Sci.,* **50,** 3894–3908.

Deardorff, J. W., 1966: The counter-gradient heat flux in the lower atmosphere and in the laboratory. *J. Atmos. Sci.,* **23,** 503–506.

Derbyshire, S. H., I. Beau, P. Bechtold, J.-Y. Grandpeix, J.-M. Piriou, J.-L. Redelsperger, and P. M. M. Soares, 2004: Sensitivity of moist convection to environmental humidity. *Quart. J. Roy. Meteor. Soc.,* **130,** 3055–3079.

De Rooy, W. C., and A. P. Siebesma, 2008: A simple parameterization for detrainment in shallow cumulus. *Mon. Wea. Rev.,* **136,** 560–576.

French, J. R., G. Vali, and R. D. Kelly, 1999: Evolution of small cumulus clouds in Florida: Observations of pulsating growth. *Atmos. Res.,* **52,** 143–165.

Grabowski, W. W., and Coauthors, 2006: Daytime convective development over land: A model intercomparison based on LBA observations. *Quart. J. Roy. Meteor. Soc.,* **132,** 317–344.

Grant, A. L. M., 2001: Cloud-base fluxes in the cumulus-capped boundary layer. *Quart. J. Roy. Meteor. Soc.,* **127,** 407–421.

——, 2006: The cumulus-capped boundary layer. II: Interface fluxes. *Quart. J. Roy. Meteor. Soc.,* **132,** 1405–1422.

Holland, J. Z., and E. M. Rasmusson, 1973: Measurement of atmospheric mass, energy, and momentum budgets over a 500-kilometer square of tropical ocean. *Mon. Wea. Rev.,* **101,** 44–55.

Holtslag, A. A. M., and C.-H. Moeng, 1991: Eddy diffusivity and countergradient transport in the convective atmospheric boundary layer. *J. Atmos. Sci.,* **48,** 1690–1698.

Kain, J. S., and J. M. Fritsch, 1990: A one-dimensional entraining/detraining plume model and its application in convective parameterizations. *J. Atmos. Sci.,* **47,** 2784–2802.

Klein, S. A., and D. L. Hartmann, 1993: The seasonal cycle of low stratiform clouds. *J. Climate,* **6,** 1587–1606.

Knight, C. A., and L. J. Miller, 1998: Early radar echoes from small, warm cumulus: Bragg and hydrometeor scattering. *J. Atmos. Sci.,* **55,** 2974–2992.

Köhler, M., 2005: Improved prediction of boundary layer clouds. *ECMWF Newsletter*, No. 104, ECMWF, Reading United Kingdom, 18–22.

Kuang, Z., and C. S. Bretherton, 2006: A mass-flux scheme view of a high-resolution simulation of a transition from shallow to deep cumulus convection. *J. Atmos. Sci.,* **63,** 1895–1909.

LeMone, M. A., and W. T. Pennell, 1976: The relationship of trade wind cumulus distribution to subcloud layer fluxes and structure. *Mon. Wea. Rev.,* **104,** 524–539.

Lock, A. P., A. R. Brown, M. R. Bush, G. M. Martin, and R. N. B. Smith, 2000: A new boundary layer mixing scheme. Part I: Scheme description and single-column model tests. *Mon. Wea. Rev.,* **128,** 3187–3199.

Mapes, B. E., 2000: Convective inhibition, subgrid-scale triggering energy, and stratiform instability in a toy tropical wave model. *J. Atmos. Sci.,* **57,** 1515–1535.

Mellor, G. L., and T. Yamada, 1974: A hierarchy of turbulence closure models for planetary boundary layers. *J. Atmos. Sci.,* **31,** 1791–1806.

Morton, B. R., G. Taylor, and J. S. Turner, 1956: Turbulent gravitational convection from maintained and instantaneous sources. *Proc. Roy. Soc. London,* **234A,** 1–23.

Neggers, R. A. J., 2009: A dual mass flux framework for boundary layer convection. Part II: Clouds. *J. Atmos. Sci.,* **66,** 1489–1506.

——, A. P. Siebesma, and H. J. J. Jonker, 2002: A multiparcel model for shallow cumulus convection. *J. Atmos. Sci.,* **59,** 1655–1668.

——, P. G. Duynkerke, and S. M. A. Rodts, 2003a: Shallow cumulus convection: A validation of large-eddy simulation against aircraft and Landsat observations. *Quart. J. Roy. Meteor. Soc.,* **129,** 2671–2696.

——, H. J. J. Jonker, and A. P. Siebesma, 2003b: Size statistics of cumulus cloud populations in large-eddy simulation. *J. Atmos. Sci.,* **60,** 1060–1074.

——, A. P. Siebesma, G. Lenderink, and A. A. M. Holtslag, 2004: An evaluation of mass flux closures for diurnal cycles of shallow cumulus. *Mon. Wea. Rev.,* **132,** 2525–2538.

——, B. Stevens, and J. D. Neelin, 2006: A simple equilibrium model for shallow-cumulus-topped mixed layers. *Theor. Comput. Fluid Dyn.,* **20,** 305–322, doi:10.1007/s00162-006-0030-1.

——, ——, and ——, 2007: Variance scaling in shallow-cumulus-topped mixed layers. *Quart. J. Roy. Meteor. Soc.,* **133,** 1629–1641.

Nicholls, S., and M. A. LeMone, 1980: The fair weather boundary layer in GATE: The relationship of subcloud fluxes and structure to the distribution and enhancement of cumulus clouds. *J. Atmos. Sci.,* **37,** 2051–2067.

Nitta, T., and S. Esbensen, 1974: Heat and moisture budget analyses using BOMEX data. *Mon. Wea. Rev.,* **102,** 17–28.

Ooyama, K., 1971: A theory on parameterization of shallow cumulus convection. *J. Meteor. Soc. Japan,* **49,** 744–756.

Rauber, R. M., and Coauthors, 2007: Rain in shallow cumuli over the ocean—The RICO campaign. *Bull. Amer. Meteor. Soc.,* **88,** 1912–1928.

Raymond, D. J., and A. M. Blyth, 1986: A stochastic mixing model for non-precipitating cumulus clouds. *J. Atmos. Sci.,* **43,** 2708–2718.

Siebesma, A. P., and J. W. M. Cuijpers, 1995: Evaluation of parametric assumptions for shallow cumulus convection. *J. Atmos. Sci.,* **52,** 650–666.

——, and J. Teixeira, 2000: An advection–diffusion scheme for the convective boundary layer: Description and 1D results. Preprints, *14th Symp. on Boundary Layer and Turbulence,* Aspen, CO, Amer. Meteor. Soc., 133–140.

——, and Coauthors, 2003: A large eddy simulation intercomparison study of shallow cumulus convection. *J. Atmos. Sci.,* **60,** 1201–1219.

——, and Coauthors, 2004: Cloud representation in general circulation models over the northern Pacific Ocean: A EUROCS intercomparison study. *Quart. J. Roy. Meteor. Soc.,* **130,** 3245–3267.

——, P. M. M. Soares, and J. Teixeira, 2007: A combined eddy-diffusivity mass-flux approach for the convective boundary layer. *J. Atmos. Sci.,* **64,** 1230–1248.

Simpson, J., and V. Wiggert, 1969: Models of precipitating cumulus towers. *Mon. Wea. Rev.,* **97,** 471–489.

Soares, P. M. M., P. M. A. Miranda, A. P. Siebesma, and J. Teixeira, 2004: An eddy-diffusivity/mass-flux parameterization for dry and shallow cumulus convection. *Quart. J. Roy. Meteor. Soc.,* **130,** 3365–3383.

Sommeria, G., and J. W. Deardorff, 1977: Subgrid-scale condensation in models of non-precipitating clouds. *J. Atmos. Sci.,* **34,** 344–355.

Stevens, B., 2006: Boundary layer concepts for simplified models of tropical dynamics. *Theor. Comput. Fluid Dyn.,* **20,** 279–304.

——, and Coauthors, 2001: Simulations of trade wind cumuli under a strong inversion. *J. Atmos. Sci.,* **58,** 1870–1891.

Stokes, G. M., and S. E. Schwartz, 1994: The Atmospheric Radiation Measurement (ARM) program: Programmatic background and design of the cloud and radiation test bed. *Bull. Amer. Meteor. Soc.,* **75,** 1201–1222.

Tiedtke, M., 1989: A comprehensive mass flux scheme for cumulus parameterization in large-scale models. *Mon. Wea. Rev.,* **117,** 1779–1800.

Tompkins, A., and Coauthors, 2004: Moist physical processes in the IFS: Progress and plans. ECMWF Tech. Memo. 452, 93 pp.

Troen, I., and L. Mahrt, 1986: A simple model of the atmospheric boundary layer: Sensitivity to surface evaporation. *Bound.-Layer Meteor.,* **37,** 129–148.

Turner, J. S., 1986: Turbulent entrainment: The development of the entrainment assumption, and its application to geophysical flows. *J. Fluid Mech.,* **173,** 431–471.

Van Ulden, A. P., and A. P. Siebesma, 1997: A model for strong updrafts in the convective boundary layer. Preprints, *12th Symp. on Boundary Layers and Turbulence,* Aspen, CO, Amer. Meteor. Soc., 257–259.

Wyant, M. C., C. S. Bretherton, H. A. Rand, and D. E. Stevens, 1997: Numerical simulations and a conceptual model of the stratocumulus to trade cumulus transition. *J. Atmos. Sci.,* **54,** 168–192.

Wyngaard, J. C., and C.-H. Moeng, 1992: Parameterizing turbulent diffusion through the joint probability density. *Bound.-Layer Meteor.,* **60,** 1–13.

——, O. R. Coté, and Y. Izumi, 1971: Local free convection, similarity, and the budgets of shear stress and heat flux. *J. Atmos. Sci.,* **28,** 1171–1182.

Yanai, M., S. Esbensen, and J.-H. Chu, 1973: Determination of bulk properties of tropical cloud clusters from large-scale heat and moisture budgets. *J. Atmos. Sci.,* **30,** 611–627.

Yin, B., and B. A. Albrecht, 2000: Spatial variability of atmospheric boundary layer structure over the eastern equatorial Pacific. *J. Climate,* **13,** 1574–1592.